Published in final edited form as:

Nature. 2019 February ; 566(7743): 259–263. doi:10.1038/s41586-019-0928-6.

Viral and metazoan poxins are cGAMP-specific nucleases that restrict cGAS-STING signaling

James B. Eaglesham[1,2,3], **Youdong Pan**[4], **Thomas S. Kupper**[4,5], and **Philip J. Kranzusch**[1,2,3,6,*]

[1]Department of Microbiology and Immunobiology, Harvard Medical School, Boston, MA 02115, USA

[2]Department of Cancer Immunology and Virology, Dana-Farber Cancer Institute, Boston, MA 02115, USA

[3]Harvard PhD Program in Virology, Division of Medical Sciences, Harvard University, Boston, MA 02115, USA

[4]Department of Dermatology and Harvard Skin Disease Research Center, Brigham and Women's Hospital, Boston, Harvard Medical School, Boston, MA 02115, USA

[5]Dana-Farber/Brigham and Women's Cancer Center, Boston, MA 02115, USA

[6]Parker Institute for Cancer Immunotherapy at Dana-Farber Cancer Institute, Boston, MA 02115, USA

Abstract

Cytosolic DNA triggers innate immune responses through activation of cyclic GMP–AMP synthase (cGAS) and production of the cyclic dinucleotide second messenger 2′3′ cGAMP[1–4]. 2′3′ cGAMP is a potent inducer of immune signaling, but no intracellular nucleases are known to cleave 2′3′ cGAMP and prevent activation of the receptor stimulator of interferon genes (STING)[5–7]. Through a biochemical screen analyzing 24 mammalian viruses, here we identify poxvirus immune nucleases (poxins) as a family of 2′3′ cGAMP-specific degrading enzymes. Poxins cleave 2′3′ cGAMP to restrict STING-dependent signaling, and deletion of the poxin gene (*B2R*) attenuates vaccinia virus replication *in vivo*. Crystal structures of vaccinia virus poxin in pre- and post-reactive states define the mechanism of selective 2′3′ cGAMP degradation through metal-independent cleavage of the 3′–5′ bond, converting 2′3′ cGAMP into linear Gp[2′–5′]Ap[3′]. Poxins are conserved in mammalian poxviruses, and remarkably, we further identify functional poxin homologues in the genomes of moths and butterflies and the baculoviruses which infect them. Baculovirus and insect host poxin homologues retain selective 2′3′ cGAMP

*Correspondence: philip_kranzusch@dfci.harvard.edu. Correspondence and requests for materials should be addressed to P.J.K.

Author Contributions: Project was conceived, and experiments were designed by J.B.E. and P.J.K. All virology, biochemical, and structural experiments were conducted by J.B.E. with assistance from P.J.K. Animal experiments were conducted by Y.P. and T.S.K. The manuscript was written by J.B.E. and P.J.K and all authors support the conclusions.

Supplementary Information is available in the online version of the paper.

Author Information: The authors have no competing financial interests to declare.

degradation activity, suggesting an ancient role for poxins in cGAS-STING regulation. Our results define poxins as a family of 2′3′ cGAMP-specific nucleases and demonstrate a mechanism for how viruses evade innate immunity.

The enzyme cGAS recognizes cytosolic DNA and synthesizes 2′3′ cGAMP to activate STING-dependent interferon and NF-κB immune responses[7]. 2′3′ cGAMP is highly stable in the cytosol of human cells, activates STING at low nanomolar concentrations, and can spread through cellular gap junctions to activate immune responses in adjacent cells[5,7]. The extracellular ATP metabolizing enzyme ENPP1 is capable of degrading 2′3′ cGAMP[6], but no cytosolic nucleases have been identified that are able to selectively target 2′3′ cGAMP and restrict cGAS-STING signaling. Using cytosolic extracts from human monocyte and kidney cells, we confirmed that 2′3′ cGAMP is highly stable with no degradation detected after 20 h of incubation (Extended Data Figure 1a). 2′3′ cGAMP activates STING to initiate antiviral responses and can be packaged into viral particles during egress[8,9]. We therefore hypothesized that strong selective pressure would exist for viruses to specifically destabilize 2′3′ cGAMP and prevent induction and spread of cGAS-STING immune responses. To test for virus-induced degradation of 2′3′ cGAMP, we designed a biochemical screen and analyzed 24 different mammalian viruses representing 13 viral families (Figure 1a,b, Supplementary Table 1). Radiolabeled 2′3′ cGAMP was completely degraded when exposed to lysate from cells infected with vaccinia virus (VACV), a member of the family *Poxviridae* (Figure 1b). VACV-infected cell lysates rapidly convert 2′3′ cGAMP into an intermediate product that is then resolved into a second, faster-migrating species on thin-layer chromatography (Figure 1c). 2′3′ cGAMP degradation activity tracked with VACV infection rather than host cell tissue or species-origin (Extended Data Figure 1b,c), suggesting that activity is derived from a viral product. We therefore named the viral factor responsible for 2′3′ cGAMP degradation pox virus immune nuclease, or poxin.

Poxviruses are large DNA viruses which replicate exclusively in the cytoplasm of infected cells and encode factors dedicated to evasion of host immune signaling[10]. To identify the VACV poxin-encoding gene, we used activity-guided fractionation to specifically enrich poxin from infected cell lysates (Figure 1d, Extended Data Figure 2). Mass-spectrometry analysis of fractions enriched using two independent purification schemes revealed that only the protein product of the VACV gene *B2R* (NCBI YP_233066.1) was highly enriched (Figure 1e). Recombinant protein robustly degraded 2′3′ cGAMP *in vitro* (Figure 1f, Extended Data Figure 3), using the same two-step reaction and broad pH optimum observed with VACV-infected cell lysates, confirming that the VACV *B2R* gene encodes poxin.

The activity of VACV poxin is exquisitely specific for 2′3′ cGAMP, and no degradation was observed using chemically related 3′–5′ linked cyclic dinucleotides (Figure 2a). This specificity suggests that poxin is specialized for evasion of cGAS-STING DNA sensing through degradation of the second messenger 2′3′ cGAMP. Consistent with this hypothesis, poxin cleavage renders 2′3′ cGAMP unrecognizable to the receptor STING (Figure 2b), and expression of VACV poxin in human cells was sufficient to restrict cGAS-dependent STING activation (Figure 2c, Extended Data Figure 4a,b). We constructed a deletion mutant virus (VACV-ΔPoxin), and confirmed that poxin is necessary for infected cell lysates to

degrade 2′3′ cGAMP (Extended Data Figure 4g). cGAS has previously been shown to be a critical factor for restriction of poxvirus replication[11–14]. To assess the impact of poxin deletion on VACV fitness *in vivo*, we next infected mice by scarification and measured viral loads in the resulting skin lesions. Although poxin is dispensable for replication in interferon-deficient cells (Extended Data Figure 4h), VACV-ΔPoxin replication in mice is more than 40-fold attenuated compared to WT (Figure 2d), demonstrating the importance of poxin function *in vivo*. No increase in IFN-β signaling was observed during VACV-ΔPoxin infection in an interferon-competent cell culture model of replication (Extended Data Figure 4i), indicating that the key function of poxin *in vivo* may relate to spread of 2′3′ cGAMP rather than prevention of interferon signaling in the primary infected cell. Together, these data define a mechanism of poxvirus cGAS-STING evasion through poxin-mediated cleavage of 2′3′ cGAMP.

To define the molecular mechanism of poxin activity, we determined a series of X-ray crystal structures of VACV poxin that correspond to the *apo* (1.7 Å), pre-reactive (2.6 Å) and post-reactive (2.1 Å) states of 2′3′ cGAMP degradation (Extended Data Table 1). VACV poxin forms a V-shaped homodimeric complex, where N-terminal protease-like domains flank a central 14-stranded beta-sandwich core created by extensive hydrophobic contacts between the C-terminal domains of each monomer (Figure 3a, Extended Data Figure 5). The pre-reactive crystal structure of VACV poxin bound to a phosphorothioate nonhydrolyzable 2′3′ cGAMP analog reveals that substrate recognition occurs in a deep pocket between the N-terminal and C-terminal domains of opposing monomers. Helix σ2 in the C-terminal domain undergoes a 4 Å movement to clamp around the captured 2′3′ cGAMP molecule (Extended Data Figure 5b). Eight poxin residues read out the base identity and unique geometry imposed by the noncanonical 2′–5′ bond, explaining the exquisite specificity of 2′3′ cGAMP recognition (Figure 3b, Extended Data Figure 6).

The 2′–5′ bond of 2′3′ cGAMP is buried in a deep pocket, and the 3′–5′ bond is presented in the poxin active site for hydrolysis (Figure 3b). Using site-specific labeling of 2′3′ cGAMP, we confirmed that degradation occurs through specific hydrolysis of the canonical 3′–5′ bond, leaving the 2′–5′ bond intact (Extended Data Figure 7a,b). Crystals of poxin grown in the presence of 2′3′ cGAMP yielded a post-reactive structure and clear density for the final product Gp[2′–5′]Ap[3′] (Extended Data 6). Notably, metal ions were not observed in these structures, and poxin activity is resistant to metal chelation (Extended Data Figure 7c). Once bound to poxin, the adenine base in 2′3′ cGAMP is rotated 60° compared to the in-solution or STING-bound conformation[15–18], resulting in a distorted 2′3′ cGAMP conformation that repositions the 2′ OH to serve as the reactive nucleophile (Figure 3c). The VACV poxin residues H17, Y138, and K142 are located proximal to the scissile 3′–5′ bond, and positioning in the active site suggests that H17 and K142 function as the general acid and base of the reaction (Figure 3b,d). Mutational analysis confirmed H17 and K142 are essential for activity, while mutation of Y138 stalls the reaction at the intermediate stage (Figure 3e). A similar catalytic triad is observed in tRNA splicing endonucleases[19] (Extended Data Figure 6c), supporting that poxin-catalyzed degradation of 2′3′ cGAMP proceeds through the conventional reaction shared between metal-independent ribonucleases[20]. In sum, these data reveal a mechanism where poxin is a metal-independent

nuclease that cleaves the canonical bond of 2′3′ cGAMP to inhibit cGAS-STING immunity.

VACV poxin does not exhibit any detectable structural homology with previously known nuclease or phosphodiesterase enzymes. Poxin is conserved in most viruses in the genus *Orthopoxvirus*, including the human pathogens monkeypox virus and cowpox virus (Figure 4a, Extended Data Figure 8a, 9a), and is sometimes fused to an additional C-terminal domain previously noted to have homology with human schlafen proteins[21]. We cloned four divergent poxin genes from members of the *Poxviridae* and each retained specific recognition of 2′3′ cGAMP and hydrolysis activity (Figure 4b, Extended Data Figure 9c). We next used the structure of VACV poxin and conservation of active-site residues to guide a bioinformatic search for divergent poxin family members outside of the *Poxviridae*. Surprisingly, this search revealed poxin homologues in the *Alphabaculovirus* genus of insect DNA viruses (p26 proteins, e.g. AcNPV P26 NCBI NP_054166.1), and poxin genes in insects of the order Lepidoptera which serve as exclusive hosts of alphabaculoviruses (HDD13 proteins, e.g. *Bombyx mori* HDD13 NCBI XP_021205460.1) (Figure 4c). Insect cellular and viral poxin homologues are enzymatically active, retain specificity for 2′3′ cGAMP degradation, and insect host poxin activity can be detected in lysates of the common cell lines *Sf*21 and Hi5 (Figure 4d,e Extended Data Figure 9c). In support of a conserved role of insect poxins in immune regulation, the STING signaling pathway is functional in insects[18,22,23] and the lepidopteran poxin gene is induced upon pathogen infection[24]. Poxviruses and baculoviruses can share overlapping host tropisms, and readily acquire genes through homologous recombination[25,26], potentially explaining how poxins evolved and spread between insects, insect viruses and mammalian pathogens (Figure 4f).

Through discovery and characterization of a 2′3′ cGAMP-specific nuclease in VACV-infected cell lysates, our data reveal a potent viral strategy for cGAS-STING pathway evasion. Poxin activity provides a mechanistic explanation for recent findings demonstrating that virulent poxviruses inhibit cGAS-STING signaling during infection at a step downstream of cGAS activation[13]. Two notable exceptions to conservation of poxin activity are Variola major virus, the causative agent of smallpox disease, and the modified vaccinia Ankara (MVA) vaccine strain which both show inactivation of poxin (Figure 4a; Extended Data Figure 8b). Inactivation of the poxin gene in Variola major virus further suggests that multiple strategies may exist in poxviruses to subvert cGAS-STING immunity[27]. Poxvirus vectors are widely used in human and animal vaccination, gene therapy, and as cancer oncolytics[28,29]. Loss of poxin resulted in significant attenuation of VACV in a mouse model of replication, indicating that modulation of cGAS-STING signaling through poxin deletion may be an important consideration in design of poxvirus-based vaccines and therapeutics. The ability of 2′3′ cGAMP to cross cellular gap-junctions[5] and infiltrate budding viral particles[8,9] provides the host an opportunity to counteract pathogen factors that inhibit cGAS-STING activation but do not completely eliminate all 2′3′ cGAMP production[30]. Through direct targeting of 2′3′ cGAMP, poxin activity is an elegant viral adaptation to prevent both activation and cellular spread of STING signaling. Conservation of poxins between mammalian viruses and insects reaffirms the ancestral roots of 2′3′ cGAMP-dependent signaling in animals[18], and underscores the wide range of host-virus conflicts that drive new mechanisms of innate immunity surveillance and evasion.

Methods

Cell lines and viruses

A549, BSC-40, BSR-T7, and Vero cells, as well as VACV (strain western reserve vTF7–3)[31] stocks were kind gifts from S. Whelan (Harvard Medical School). THP-1 cells and 293T cells were purchased from ATCC. All cell lines were maintained in Dulbecco's Modified Eagle Media (DMEM) (VWR) supplemented with 10% fetal bovine serum (FBS) (VWR, Seradigm), with the exception of THP-1 cells which were maintained in RPMI-1640 medium (Life Technologies) supplemented with 10% FBS and 50 nM β-mercaptoethanol. Infections with VACV were performed for 1 h in 1× PBS supplemented with 1 mM $CaCl_2$ and 1 mM $MgCl_2$. After 1 h, excess virus was aspirated, and cells were either harvested (1 hpi) or infection was allowed to continue in DMEM supplemented with 2.5% FBS and 50 mM HEPES-NaOH pH 7.5 until harvest at stated time points. Infected cells were washed once in 1× PBS, scraped into 1× PBS, collected by centrifugation, and lysed in 1% NP-40, 20 mM HEPES-NaOH pH 7.5, 150 mM NaCl, 1 mM TCEP-KOH to prepare virus-infected cell lysates. Infections with other viruses were performed according to details in Supplementary Table 1. *Sf*21 and Hi5 insect cells were kind gifts from R. Ross and S. Harrison (Harvard Medical School). Spinner cultures of insect cells were maintained in TC100 media (Gibco) supplemented with 10% FBS, harvested by centrifugation, and lysed with the same lysis buffer as above. VACV was propagated in Vero cells, and plaque assays were performed in Vero cells, according to published protocols[32].

Synthesis of cyclic dinucleotides

2′3′ cGAMP for downstream degradation assays was produced using recombinant mouse cGAS. Recombinant human SUMO2-tagged mouse cGAS was purified from *E. coli* using Ni-NTA affinity, digested with human SENP2 protease, and further purified with heparin ion-exchange and S75 size exclusion chromatography as previously described[33]. Mouse cGAS (14 μM) was incubated for 20 h at 37 °C with either 200 μM ATP and 200 μM GTP (high substrate) or 25 μM each (low substrate) in the presence of 1 μM 45 bp stimulatory dsDNA in 20 μl buffer composed of 50 mM HEPES-KOH pH 7.5, 5 mM $Mg(OAc)_2$, 60 mM KCl, and 1 mM DTT. Reactions were trace labeled with [α^{32}P] GTP (Perkin Elmer) except in Extended Data Figure 7a where indicated reactions were labeled with [α^{32}P] ATP. After completion, reactions were treated with Antarctic Phosphatase (NEB) for 20 min to digest remaining labeled nucleoside triphosphates, and heat inactivated at 65 °C for 20 min before direct use in downstream poxin activity assays. 3′–5′ linked cyclic dinucleotides were enzymatically synthesized in a similar manner using recombinant *Vibrio cholerae* DncV incubated with either ATP and GTP (3′3′ cGAMP synthesis), GTP alone (c-di-GMP synthesis), or ATP alone (c-di-AMP synthesis) as previously described[18,34]. All 3′–5′ linked cyclic dinucleotides were prepared with 200 μM of each required NTP, except in Extended Data Figure 9c where synthesis was performed with 25 μM of each NTP.

2′3′ cGAMP used for crystallography was enzymatically synthesized by 24 h incubation at 37 °C of 100 nM recombinant mouse cGAS with 500 μM each ATP and GTP, in the presence of 50 μg ml^{-1} salmon sperm DNA in 500 ml buffer composed of 10 mM Tris-HCl pH 7.5, 12.5 mM NaCl, 10 mM $MgCl_2$, 1 mM DTT. 2′3′ cGAMP was subsequently

purified by ion exchange (2× 5ml HiTrap Q columns) on a gradient of 0–2 M NH_4OAc, and lyophilized. Freeze dried 2′3′ cGAMP was washed twice with methanol before final lyophilization and storage as powder at −20 °C.

Poxin activity assays

Degradation of 2′3′ cGAMP was assessed by incubation of cell lysates or recombinant protein in the presence of either ~20 μM 2′3′ cGAMP (high substrate) or ~2.5 μM 2′3′ cGAMP (low substrate) in 10 μl buffer composed of 50 mM HEPES-KOH pH 7.5, 35 mM KCl, and 1 mM DTT. High substrate 2′3′ cGAMP was used in all degradation assays except those displayed in Figure 1b, Figure 4b,d,e, Extended Data Figures 1a and 9c where low substrate was used to allow more sensitive detection of 2′3′ cGAMP degradation. For the virus lysate screen in Figure 1b, ~30 ng of each virus-infected cell lysate was incubated in a 10 μl reaction with ~2.5 μM 2′3′ cGAMP for 20 h at 37 °C. In all further experiments with VACV-infected cell lysates, 100 ng VACV-infected cell lysate was used in each reaction. In experiments with *Sf*21 and Hi5 lepidopteran cell lysates, 1 μg lysate was used in each reaction. Recombinant poxin protein activity assays were carried out at a final concentration of 100–400 nM poxin. Unless otherwise stated, reactions were carried out for 5–15 min before resolution of degradation products on a PEI-cellulose thin-layer chromatography (TLC) plate (Millipore) in a solvent composed of 1.5 M KH_2PO_4 pH 3.8. After developing, TLC plates were dried and exposed to a phosphor screen overnight and imaged on a Typhoon phosphor-imager (GE).

Virus lysate screen

Infections with diverse viruses were carried out by collaborating labs according to the conditions listed in Supplementary Table 1. Infected cells were harvested and stored at −80ºC before lysis in 1% NP-40, 20 mM HEPES-KOH pH 7.5, 150 mM NaCl, and 1 mM TCEP-KOH. Cytoplasmic extracts were generated by collecting the supernatant fraction following centrifugation of whole cell lysates at 22,000 × g for 10 min. Lysate concentrations were quantified using a Bradford assay, and normalized accordingly before poxin activity assays as described above.

Poxin biochemical fractionation and identification

Poxin was enriched and identified directly from infected cell lysates. 16× T150 flasks of BSC-40 cells were infected at an MOI of 5. After 6 h, cells were scraped into 1× PBS, collected by centrifugation, and stored at −80 °C. The resulting infected material was split into two portions, lysed and fractionated with either an ion exchange (IEX)-based or a hydrophobic-interaction chromatography (HIC)-based purification. Cells were lysed in 1% NP-40, 20 mM HEPES-KOH pH 7.5, 150 mM NaCl, 1 mM DTT and cytosolic lysates were collected from the supernatant fractions following centrifugation at 22,000 × g for 10 min. Resulting cytoplasmic extracts were fractionated by IEX using a 1 ml HiTrap Q HP column and a gradient from 0.05–1 M NaCl. Fractions with poxin activity were pooled and further purified on a 10/300 S200 size exclusion column (GE). Alternatively, cytoplasmic extracts were subjected to a 30% $(NH_4)_2SO_4$ cut at 4 °C for 1 h with gentle spinning, and centrifuged at 50,000 × g for 15 min. Clarified supernatant was loaded on a 1 ml HiTrap Phenyl HIC column (GE), and eluted using a gradient of 1.2–0 M $(NH_4)_2SO_4$ in a buffer

containing constant 150 mM NaCl. Enriched fractions with poxin activity were then further fractionated on a 10/300 S75 size exclusion column (GE). After each purification step, 1 μl of each fraction was tested for poxin activity as described above, and active fractions were pooled for additional purification. After IEX and size exclusion, the single fraction with peak activity and inactive background fractions that eluted before and after poxin activity were analyzed with mass spectrometry. Additionally, a single active fraction was selected for analysis after HIC and size exclusion. Mass spectrometry protein analysis and label-free quantification of the IEX samples were performed at the Harvard Medical School Taplin Facility.

Recombinant protein purification

The VACV poxin gene *B2R* was PCR-amplified from purified viral DNA and cloned into a custom pET vector designed to express a 6×His-tagged N-terminal human SUMO2 fusion[33]. Poxin homologues were cloned using synthetic DNA fragments (IDT) and HiFi gibson assembly (NEB). Recombinant poxin proteins were expressed in *E. coli* BL21 RIL bacteria (Agilent) using 50 ml starter cultures grown in MDG media, and 2× 1 L induction cultures grown in M9ZB media as previously described[33]. Alternatively, MPXV poxin starter and induction cultures were grown with 2YT media as previously described[34]. Selenomethionine-substituted (SeMet) VACV poxin was grown in overnight MDG starter cultures, and in 2× 1 L induction cultures of altered M9ZB medium containing 40% glucose as a sole carbon source, supplemented with 1 μg ml^{-1} thiamine. SeMet M9ZB cultures were grown to an OD of ~0.6 before addition of the following amino acids for selenomethinonine labeling and suppression of methionine biosynthesis: 50 mg L^{-1} leucine, isoleucine, and valine (VWR); 100 mg L^{-1} phenylalanine, lysine, and threonine (VWR); 75 mg L^{-1} selenomethionine (Acros Organics). Cultures were allowed to grow for an additional 20 min at 37 °C with shaking at 230 RPM, and then transferred to an ice bath for 20 min. Cultures were then supplemented with addition of 0.5 mM IPTG and incubated at 16 °C with shaking at 230 RPM for overnight growth. Harvested cells were disrupted by sonication in lysis buffer (20 mM HEPES-KOH pH 7.5, 400 mM NaCl, 30 mM imidazole, 10% glycerol, 1 mM DTT), and poxin proteins were purified from clarified lysates at 4 °C using Ni-NTA resin (Qiagen) and gravity chromatography. Ni-NTA resin was washed with lysis buffer supplemented to 1 M NaCl, and eluted with lysis buffer supplemented to 300 mM imidazole. The elution fraction was supplemented with ~250 μg of human SENP2 protease (fragment D364–L589 with M497A mutation)[35], and dialyzed overnight at 4 °C in dialysis buffer (20 mM HEPES-KOH pH 7.5, 300 mM NaCl, 1 mM DTT). Untagged poxin was further purified using 16/600 S75 size exclusion chromatography (GE) in 20 mM HEPES-KOH pH 7.5, 250 mM KCl, 1 mM TCEP-KOH. Final protein was concentrated to ~10–35 mg ml^{-1}, flash-frozen in liquid nitrogen and stored at −80 °C for crystallography. Alternatively, proteins for biochemistry analysis were supplemented with 10% glycerol prior to −80 °C storage. Poxin mutants tested in Figure 3 and poxin homologues tested in Figure 4 and Extended Data Figure 9 were purified as SUMO2-fusions, and dialyzed directly into storage buffer without SENP2 digestion.

STING EMSA

Human STING–cyclic dinucleotide electrophoretic mobility shift assays were performed as previously described[18]. Briefly, ~500 nM of ^{32}P radiolabeled 2′3′ cGAMP or poxin-treated 2′3′ cGAMP was incubated in a 10 μl reaction with ~20 μM human STING N154–V341 (wt R232) in 1× reaction buffer (50 mM Tris-HCl pH 7.5, 5 mM $Mg(OAc)_2$, 70 mM KCl, 1 mM TCEP-KOH) for 30 min at 25 °C. Reactions were supplemented with loading dye (6×: 40% sucrose, 0.05% xylene cyanol), and separated on a 6% non-denaturing polyacrylamide gel (7.2 cm tall, prepared with 29:1 acrylamide:bis-acrylamide and 0.5× TBE buffer) run at 100 V for 45 min with 0.5× TBE running buffer. The gel was incubated in fixing reagent (10% acetic acid, 40% methanol) for 30 min and then dried at 80 °C before exposure to a phosphor screen and imaging on a Typhoon phosphor-imager (GE).

Poxin stable cell lines and cell-based IFN-β reporter assays

HA-tagged WT VACV poxin and a catalytically inactive VACV poxin mutant H17A were cloned into the lentiviral transduction vector pN103[36]. Lentivirus was prepared as previously described[36], and lentivirally transduced HEK 293T cells were selected with 1 μg ml^{-1} puromycin for two passages before removal of selection. Luciferase assays were performed as previously described[37]. Briefly, 293T-Poxin and 293T poxin H17A (– control) cells were transfected with Lipofectamine 2000 in 96-well plates with: a control pRL plasmid encoding *Renilla* luciferase under a constitutive promoter (2 ng), a pIFN-β FLuc reporter plasmid encoding firefly luciferase under the IFN-β promoter (20 ng), a pcDNA4 plasmid encoding human STING WT allele R232 (10 ng), and either empty vector, or a pcDNA4 plasmid encoding full length human cGAS (1 ng). Luciferase activity was quantified after 18 h, and firefly luciferase activity was normalized to the *Renilla* luciferase control. Fold reporter induction was calculated by dividing the luciferase activity observed with human cGAS by background activity observed with the empty vector transfection.

Selection and validation of poxin knockout virus

Selection of poxin knockout virus was performed as previously described[38]. A cassette encoding the *super-folding GFP* (*sfGFP*) gene[39] flanked by 250 base pair homology arms identical to the VACV genome upstream and downstream of *B2R* was cloned into a pcDNA4 vector. The cassette was amplified by PCR to create linear homologous recombination template DNA. BSR-T7 cells in 6-well dishes were infected at MOI 0.05 with VACV (strain Western Reserve vTF7–3) as above, and after 1 h virus binding, inoculum was aspirated and replaced with DMEM supplemented with 2.5% FBS, before immediate transfection with 2 μg of linear homologous recombination template. 48 h later, cells were scraped into media, collected by centrifugation, re-suspended in DMEM with 2.5% FBS, and lysed by three freeze-thaw cycles, vortexing and sonication. The resulting stock was plaque-purified on Vero cells by coring sfGFP-positive plaques and transferring into DMEM with 2.5% FBS. VACV-ΔPoxin virus was purified through three iterative rounds of sfGFP-positive plaque purification, before viral stocks were prepared for use in downstream experiments. Viral stocks were used as PCR template as previously described[40], and amplicons encompassing the entire poxin *B2R* locus extending through homologous recombination junctions were verified by Sanger sequencing (Extended Data Figure 4e).

Measurement of virus interferon induction by q-RT-PCR

A549 cells were infected at an MOI of 5 with WT VACV or VACV-ΔPoxin and lysed 5 hpi. As a positive control, cells were permeabilized for 30 min with digitonin buffer (10 μg ml^{-1} digitonin, 50 mM HEPES-KOH pH 7.5, 100 mM KCl, 3 mM $MgCl_2$, 0.1 mM DTT, 85 mM sucrose, 0.2% BSA, 1 mM ATP, and 0.1 mM GTP) and stimulated with or without 25 μM 2′3′ cGAMP as previously described[41]. After stimulation, the cells were washed once with DMEM supplemented with 10% FBS, media was replaced, and cells were incubated 5 h before lysis. Infected or stimulated cells were lysed directly in TRIzol reagent (Life Technologies), and RNA was extracted according to manufacturer's instructions. Reverse transcription was carried out in a buffer composed of 25 mM Tris-HCl pH 8.4, 37.5 mM KCl, and 1.5 mM $MgCl_2$ using MMLV-M5 reverse transcriptase[42]. qPCR was performed using LUNA qPCR mix (New England Biolabs) according to manufacturer's instructions, with a final concentration of 500 nM each forward and reverse primer. Quantification was performed using the ΔΔCt method, normalizing to GAPDH. Primers were as follows: GAPDH: (forward) 5′-TTC GAC AGT CAG CCG CAT CTT CTT-3′ and (reverse) 5′-CAG GCG CCC AAT ACG ACC AAA TC-3′, IFN-β: (forward) 5′-CAG CAG TTC CAG AAG GAG GA-3′ and (reverse) 5′-AGC CAG GAG GTT CTC AAC AA-3′, CXCL10: (forward) 5′-CCA GAA TCG AAG GCC ATC AA-3′ and (reverse) 5′-CCT TTC CTT GCT AAC TGC TTT CAG-3′.

In vivo VACV replication and determination of tissue viral load

Wild-type (WT) C57BL/6 mice were purchased from Jackson Laboratory and maintained through routine breeding in the animal facility of Harvard Institutes of Medicine, Harvard Medical School. Animal experiments were performed in accordance with the guidelines put forth by the Center for Animal Resources and Comparative Medicine at Harvard Medical School, and all protocols and experimental plans received prior approval from the HMS IACUC. Mice were randomly assigned to each group before start. Experimental groups of 7-week old female mice (n=5 mice per group) were infected with either WT VACV or VACV-ΔPoxin. The sample size was chosen based on a previously published protocol to ensure sufficient statistical power[43,44]. Mice were infected by skin scarification with 1×10^6 plaque-forming units (PFU), then at 8 days after viral infection, VACV load was evaluated by q-RT-PCR as described previously[43,44]. In brief, inoculated skin samples were harvested and DNA was purified with the DNeasy Mini Kit (Qiagen) according to the manufacturer's protocol. RT-PCR was performed with the Bio-Rad iCycler iQ Real-Time PCR Detection System (Bio-Rad Laboratories). The primers and TaqMan probe used in the quantitative PCR assay are specific for the ribonucleotide reductase *I4L*. The sequences are (forward) 5′-GAC ACT CTG GCA GCC GAA AT-3′; (reverse) 5′-CTG GCG GCT AGA ATG GCA TA-3′; (probe) 5′-AGC AGC CAC TTG TAC TAC ACA ACA TCC GGA-3′. The probe was 5′-labeled with FAM and 3′-labeled with TAMRA (Applied Biosystems, Foster City, CA). Amplification reactions were performed in a 96-well PCR plate (Bio-Rad Laboratory) in a 20 μl volume containing 2× TaqMan Master Mix (Applied Biosystems), 500 nM forward primer, 500 nM reverse primer, 150 nM probe, and the template DNA. Thermal cycling conditions were 50 °C for 2 min and 95 °C for 10 min for one cycle, followed by 45 cycles of amplification (94 °C for 15 s and 60 °C for 1 min). To calculate the viral load, a standard curve was established from DNA of a VACV stock with previously determined

titer. Corresponding CT values obtained by the real-time PCR methods were plotted on the standard curve to estimate viral load in the skin samples. Comparisons for two groups were calculated using Student's t test (two tailed). Blinding was not performed during data collection or analysis, as results were based on quantitative assessment of viral load.

Crystallization and structure determination

VACV poxin crystals were grown by hanging drop vapor diffusion at 18 °C. SeMet-labeled VACV poxin was crystallized in *Apo* form, and native VACV poxin crystals were grown in complex with the phosphorothioate nonhydrolyzable analog of 2′3′ cGAMP (c[G(2′, 5′)pS(R)-A(3′,5′)pS(S), stereoisomer 1] (Biolog) yielding a pre-reactive structure, or in complex with native 2′3′ cGAMP, yielding a post-reactive structure. SeMet-substituted *Apo* VACV poxin crystals grew in 100 mM HEPES-NaOH pH 7.0, 20–22% PEG-2000 MME and cryoprotected by the addition of 20% ethylene glycol. Native VACV poxin crystals were grown with 300 μM nonhydrolyzable 2′3′ cGAMP, or with 3.3 mg ml^{-1} purified 2′3′ cGAMP in 100 mM NaOAc pH 4.8, 10–11% PEG-20,000 and cryoprotected by the addition of 30% ethylene glycol. X-ray diffraction data were collected at the Advanced Light Source (beamline 8.2.1) and the Advanced Photon Source (beamlines 24-ID-C and 24-ID-E).

X-ray crystallography data were processed with XDS and AIMLESS[45] using the SSRL *autoxds* script (A. Gonzalez, Stanford SSRL). Experimental phase information for VACV poxin was determined using data collected from SeMet-substituted crystals. 35 sites were identified with HySS in PHENIX[46], and an initial map was produced using SOLVE/RESOLVE[47]. Model building was performed using Coot[48], prior to refinement in PHENIX. The 1.7 Å SeMet *Apo* VACV poxin structure was subsequently used as a molecular replacement search model for determination of pre-reactive and post-reactive native VACV poxin structures. Final structures were refined to stereochemistry statistics for Ramachandran plot (favored / allowed), rotamer outliers, and MolProbity score as follows: VACV poxin *Apo*, 97.65% / 2.35%, 0.15% and 1.23; VACV Poxin pre-reactive state, 96.14% / 3.7%, 1.15% and 1.58; VACV poxin post-reactive state 97.93% / 2.07%, 0.72% and 1.15.

Bioinformatics and poxin homologue identification

Position-specific iterative BLAST (PSI-BLAST) search was used to identify homologues of VACV poxin, using default settings (BLOSUM62 matrix, Gap Costs: Existence 11, Extension 1, conditional compositional score matrix adjustment). All significant (E value less than 0.05) sequences that contained the known VACV poxin active site and key structural residues were selected after each PSI-BLAST round (up to 500) for refinement of the substitution matrix in each additional PSI-BLAST round. After a single PSI-BLAST round, poxvirus sequences were identified. Refinement of the substitution matrix by a further round (2 total rounds) allowed identification of baculovirus p26 proteins, and a third round identified lepidopteran host HDD13 proteins as homologues of VACV poxin. Using alignments to VACV poxin and the crystal structure, full-length homologue sequences possessing putative catalytic residues were selected for recombinant production, and biochemical poxin activity assays.

Statistics and reproducibility

Most biochemistry experiments are representative of at least 3 independent experiments, with select experiments representative of 2 independent experiments: virus lysate screen (Figure 1b), poxin fractionation and mass-spectrometry analysis (Figure 1d,e), STING gel-shift interactions (Figure 2b), PCR validation of VACV-ΔPoxin (Extended Data Figure 4d), VACV-ΔPoxin growth curves (Extended Data Figure 4h) and VACV-ΔPoxin interferon q-RT-PCR experiments (Extended Data Figure 4i). Mice scarification experiments were performed with a sample size previously determined to ensure sufficient statistical power[43,44]. All other experimental replicate details are listed in the Extended Data Figure legends.

Data Availability Statement:

Coordinates and structure factors of the VACV Poxin *Apo* and Poxin–2′3′ cGAMP complexes have been deposited in PDB under accession codes 6EA6, 6EA8, and 6EA9. All other data are available in the manuscript or the supplementary materials.

Extended Data

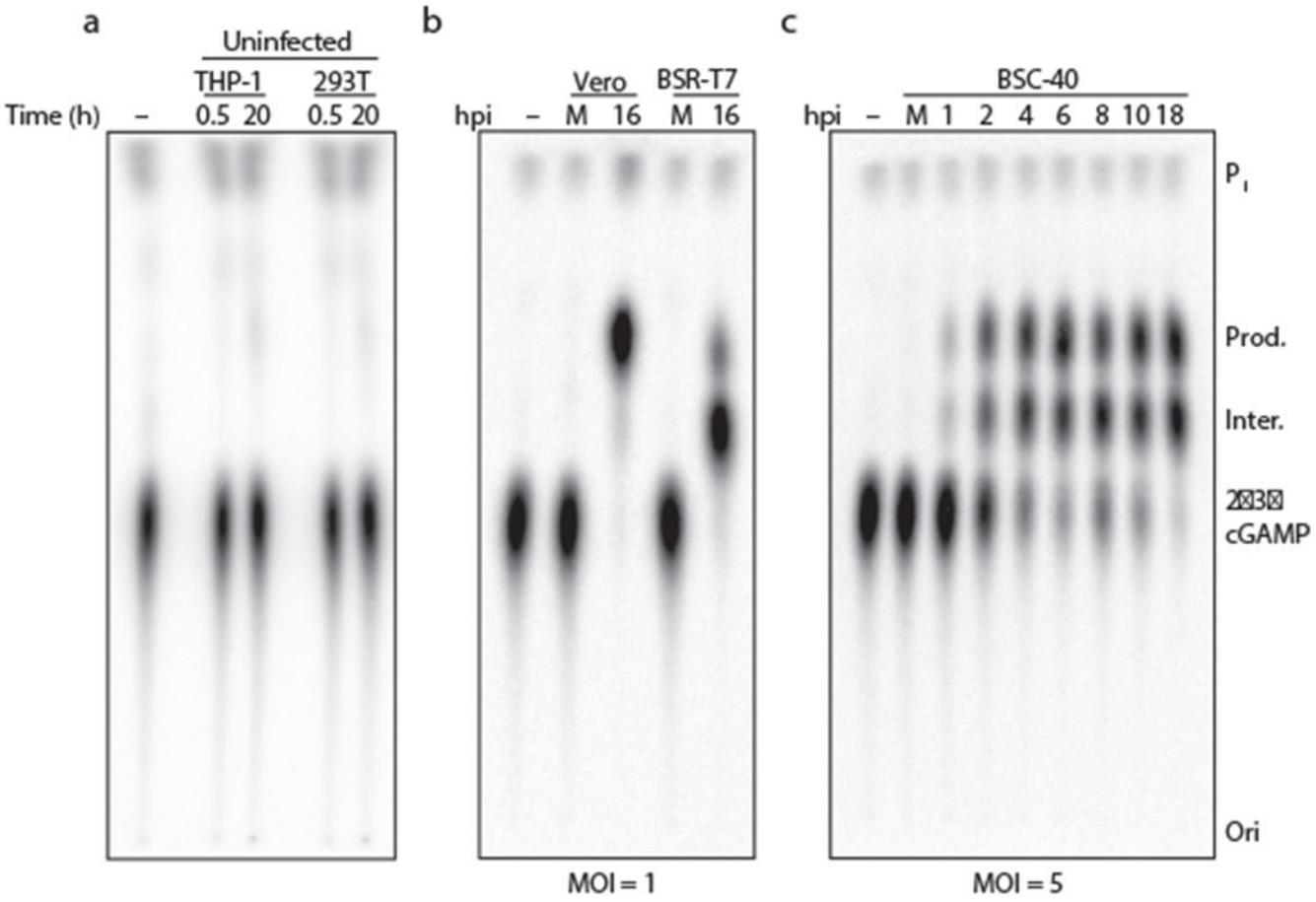

Extended Data Figure 1 |. VACV-induced 2′3′ cGAMP degradation is cell line and tissue-type independent.

a, TLC analysis of the stability of 2′3′ cGAMP (3′–5′ bond radiolabeled) following incubation in human monocyte (THP-1) or kidney (293T) cytosolic lysates. 2′3′ cGAMP is highly stable with no degradation detected after >20 h of incubation. **b**, TLC analysis of VACV-induced 2′3′ cGAMP degradation. Lysates prepared from African green monkey (*Chlorocebus aethiops*, Vero) and Golden hamster (*Mesocricetus auratus*, BSR-T7) cells each exhibit 2′3′ cGAMP degradation activity after infection with VACV, but not after mock infection (M). **c**, Time-course analysis of 2′3′ cGAMP degradation activity following infection of BSC-40 cells (*Chlorocebus aethiops*) with VACV. 2′3′ cGAMP degradation activity is detectable early <1 h after infection and persists beyond 18 h post-infection. All data are representative of 3 independent experiments.

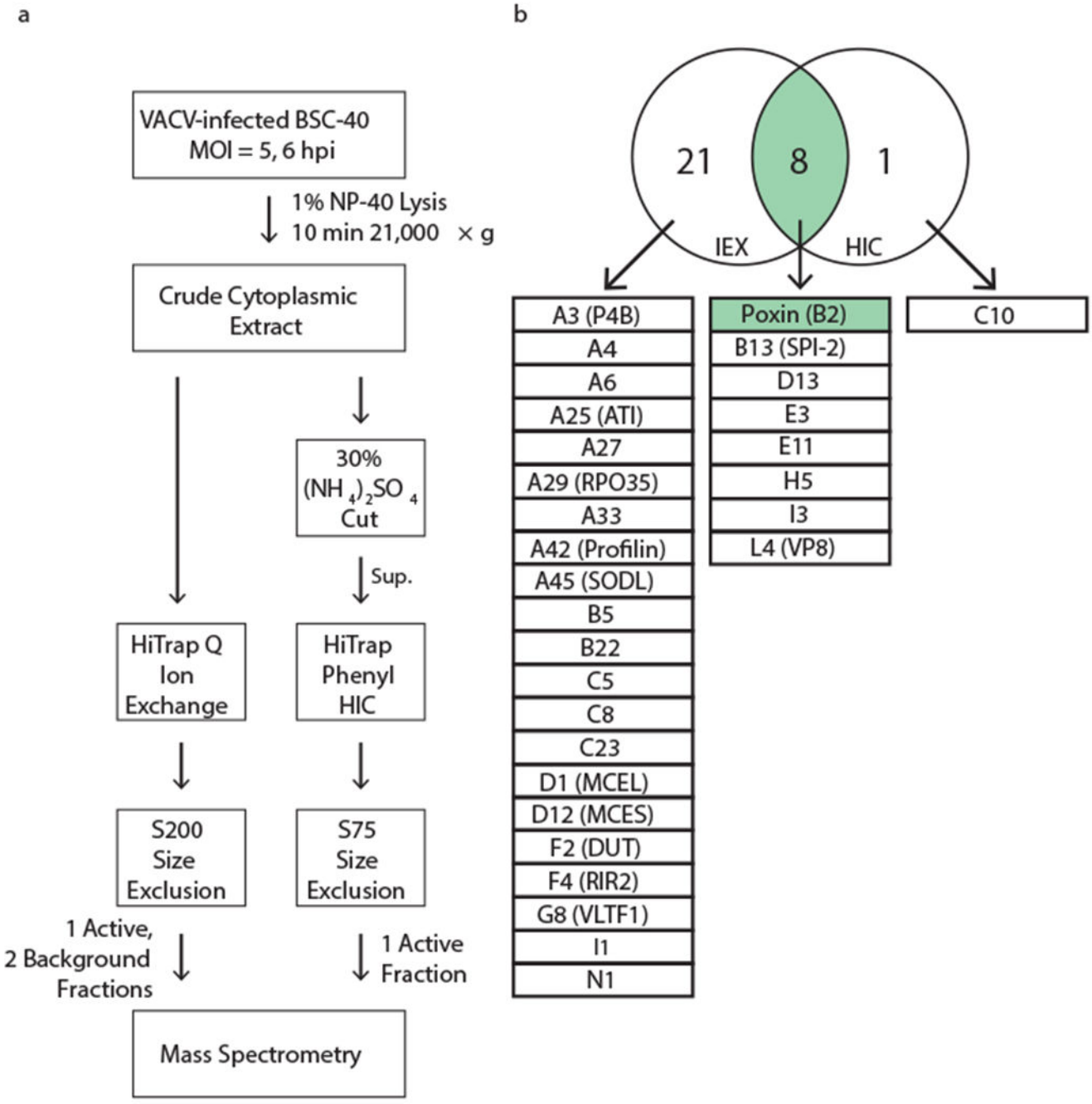

Extended Data Figure 2 |. Biochemical fractionation and mass spectrometry identification of VACV poxin.

a, Schematic of purification process developed to enrich VACV poxin from infected cell lysates. Lysates were fractionated using Q ion exchange and S200 size exclusion chromatography (purification scheme 1, left), or ammonium sulfate precipitation followed by phenyl hydrophobic interaction and S75 size exclusion chromatography (purification scheme 2, right). Fractions were tested for 2′3′ cGAMP degradation activity at each stage of purification and active fractions were pooled for subsequent purification steps. Fractions with peak activity after size exclusion were analyzed with mass spectrometry. Fold-

enrichment of proteins in the IEX active fraction compared to two inactive fractions was calculated using label-free mass spectrometry quantitation. **b**, List of VACV proteins identified in each purification scheme. VACV poxin is encoded by the *B2R* gene (green).

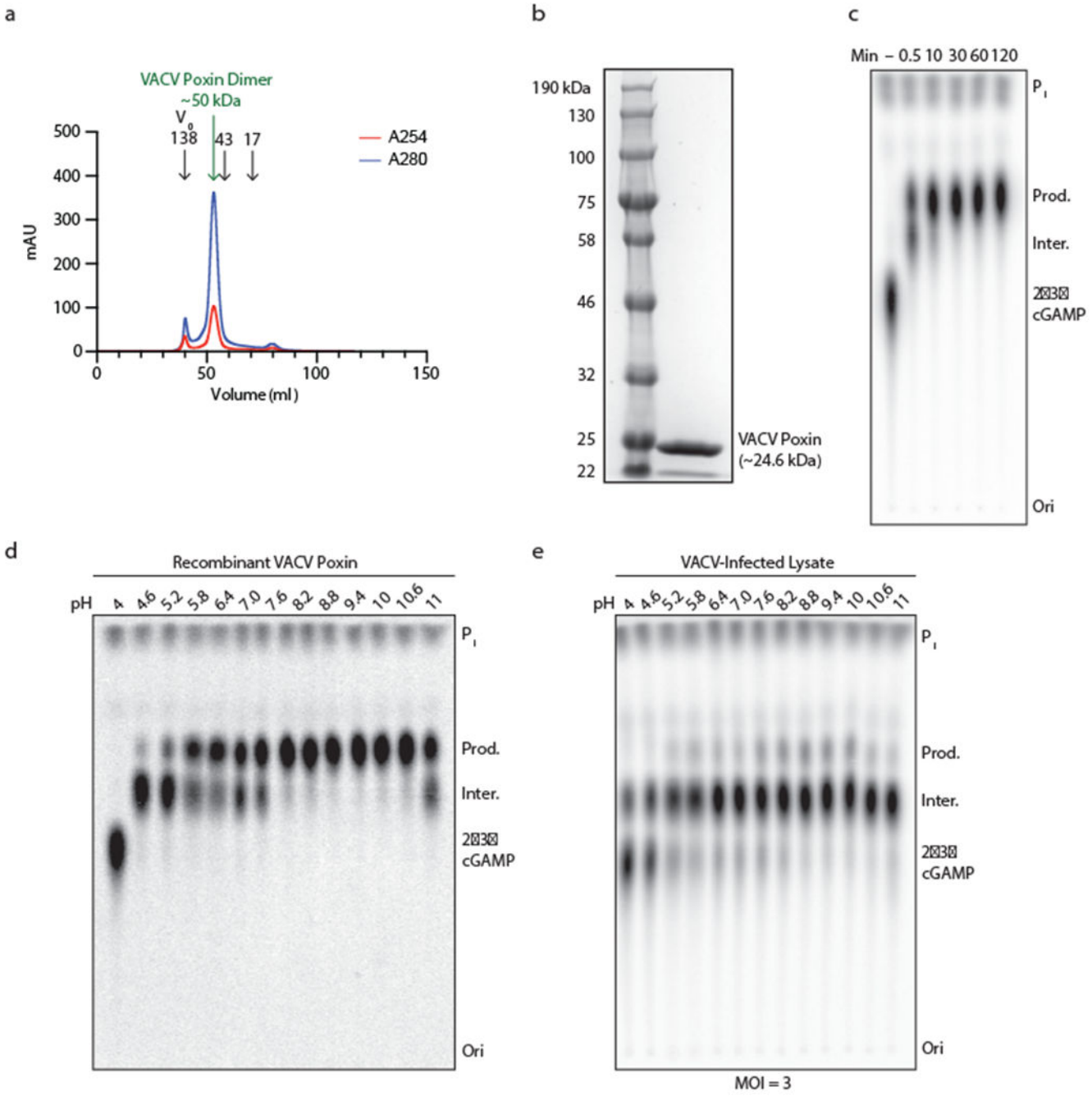

Extended Data Figure 3 |. Purification and biochemical characterization of VACV poxin.

a, Purification of recombinant VACV poxin from *E. coli*. VACV poxin was expressed as an N-terminal 6×His-SUMO fusion, the tag was proteolytically removed, and VACV poxin was isolated using S75 size exclusion chromatography. VACV poxin migrates at ~50 kDa, consistent with a homodimeric complex. **b**, SDS-PAGE coomassie stain analysis of purified recombinant VACV poxin. **c**, Reaction time-course analysis of recombinant VACV poxin 2′3′ cGAMP degradation activity. VACV poxin rapidly cleaves 2′3′ cGAMP through a slower migrating intermediate product, identical to the activity observed in VACV infected

cell lysates. Data are representative of 3 independent experiments. **d**,**e**, pH titration of recombinant VACV poxin and VACV infected cell lysate 2′3′ cGAMP degradation activity. Recombinant VACV poxin and VACV infected cell lysates share an alkaline pH optimum of 8.2–10.6. Data are representative of 3 independent experiments.

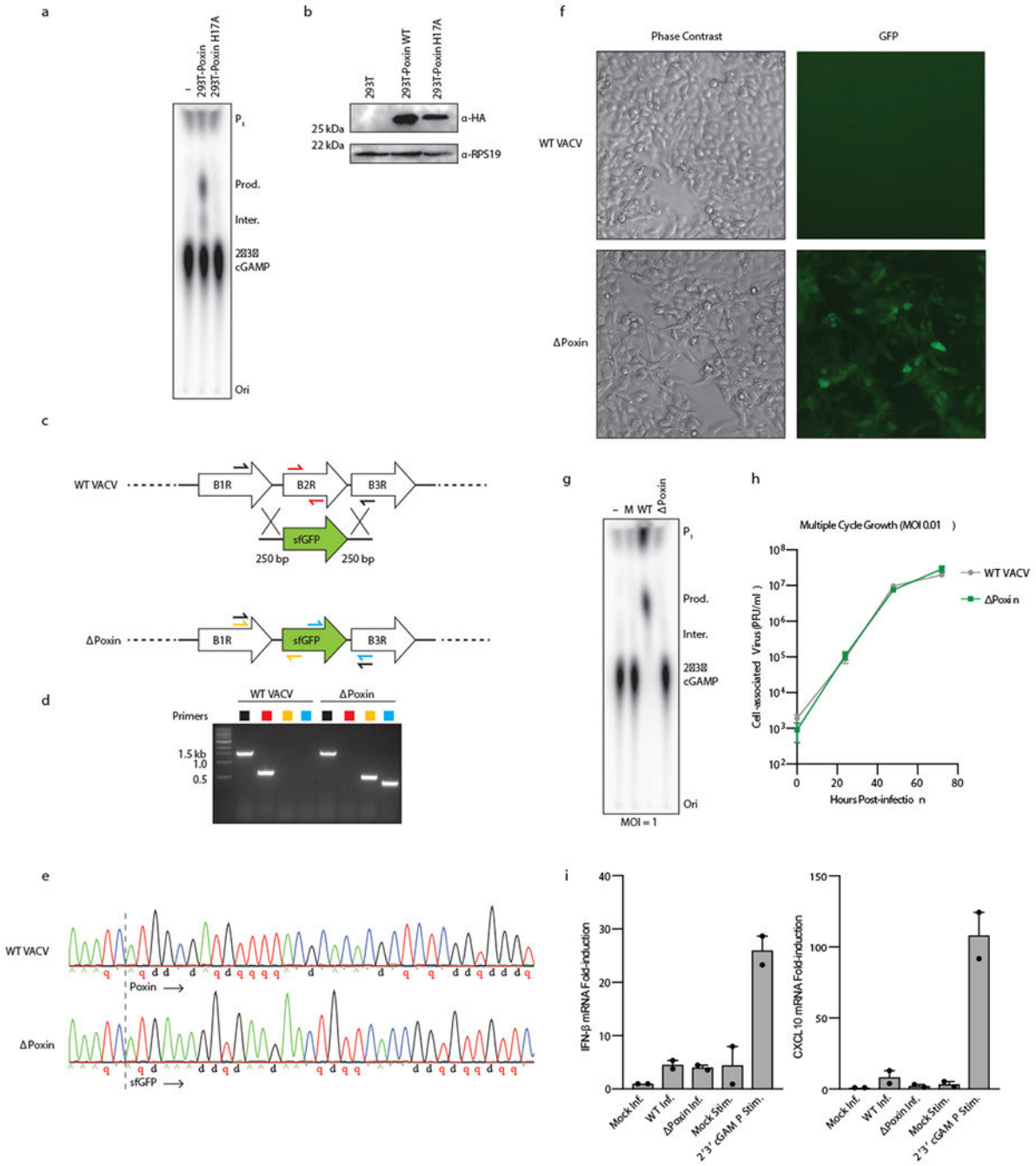

Extended Data Figure 4 |. Construction and validation of poxin-expressing cells, and poxin knockout virus.

a, TLC analysis of lysates from 293T cells after transduction with poxin WT or H17A catalytic mutant constructs, and selection with puromycin. 293T-Poxin WT cells but not control cells show degradation of 2′3′ cGAMP after a 1 h reaction. Data are representative of 2 independent experiments. **b**, Western blot analysis of poxin transduced cell lines demonstrating expression of both WT and H17A VACV poxin proteins. Data are representative of 2 independent experiments. **c**, Schematic demonstrating strategy for poxin

(*B2R*) knockout by homologous recombination and replacement with sfGFP. Colored arrows depict primers used for PCR and sequencing validation of selected viral clones. **d**, PCR analysis of parental VACV and VACV-ΔPoxin confirming removal of *B2R* and replacement with *sfGFP* gene. Data are representative of 2 independent experiments. **e**, Sequencing trace confirming replacement of *B2R* with *sfGFP* in the genome of VACV-ΔPoxin. **f**, Phase contrast and fluorescence microscopy showing Vero cells infected with WT or VACV-ΔPoxin after 20 h at MOI 1. VACV-ΔPoxin infected cells express sfGFP. Data are representative of 3 independent experiments. **g**, TLC analysis of 2′3′ cGAMP after incubation with lysates of cells infected with WT or ΔPoxin viruses. VACV-ΔPoxin infected cells lack detectable 2′3′ cGAMP degradation activity. Data are representative of 3 independent experiments. **h**, Multiple cycle growth curve (MOI 0.01) of WT and ΔPoxin VACV strains in Vero cells, demonstrating poxin knockout has no effect on viral growth kinetics in interferon-deficient cells in cell culture (n=2). Each point represents the mean with error bars representing the SEM. **i**, q-RT-PCR analysis of IFN-β and interferon stimulated gene (CXCL10) transcriptional induction following infection of A549 cells with WT or VACV-ΔPoxin after 5 h at MOI 5 (n=2). Poxin deletion does not increase IFN-β-dependent signaling in cell culture under these conditions. As a positive control, STING-dependent signaling in A549 cells was stimulated with 2′3′ cGAMP and digitonin-permeabilization.

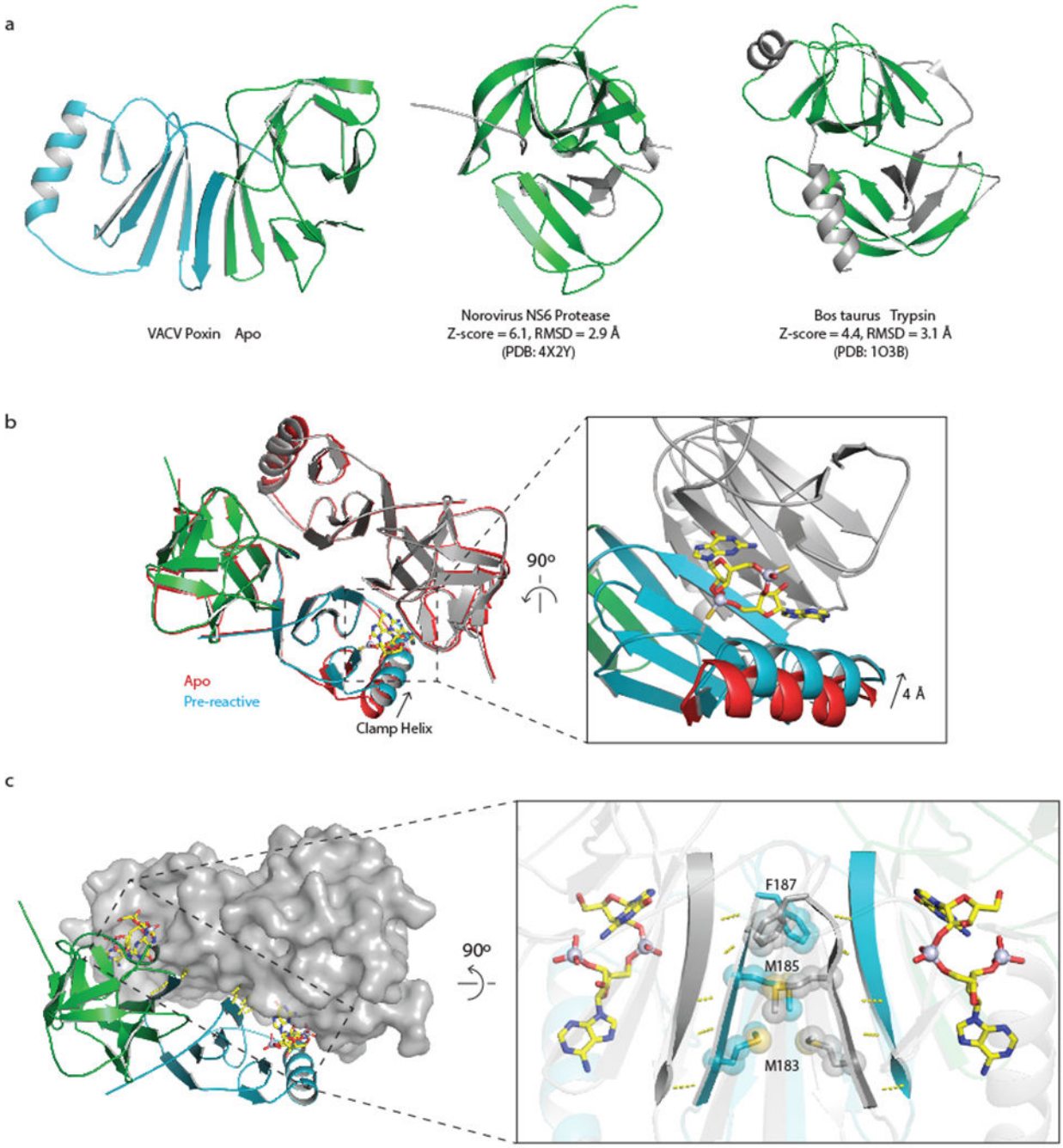

Extended Data Figure 5 |. Structural analysis of VACV poxin.

a, VACV poxin consists of two domains and homodimerizes to form the active complex. The N-terminal domain (green) has structural homology to viral 3C-like proteases (RMSD 2.9 Å). The norovirus NS6 protease and *Bos taurus* trypsin protease are colored in green and presented in the same orientation for comparison[49,50], and Z-scores were obtained from the DALI server[51]. The VACV poxin C-terminal domain (cyan) has no known structural homologues. **b**, Overlay of the *Apo* (red) and 2′3′ cGAMP bound pre-reactive (green/cyan/gray) poxin structures. 2′3′ cGAMP binding induces a 4 Å movement of the clamp helix

and repositions the active site for 3′–5′ bond hydrolysis. **c**, VACV poxin dimerization is mediated by antiparallel β-strand hydrogen bonding between monomers, as well as side chain interactions within a hydrophobic core composed of M183, M185, and F187.

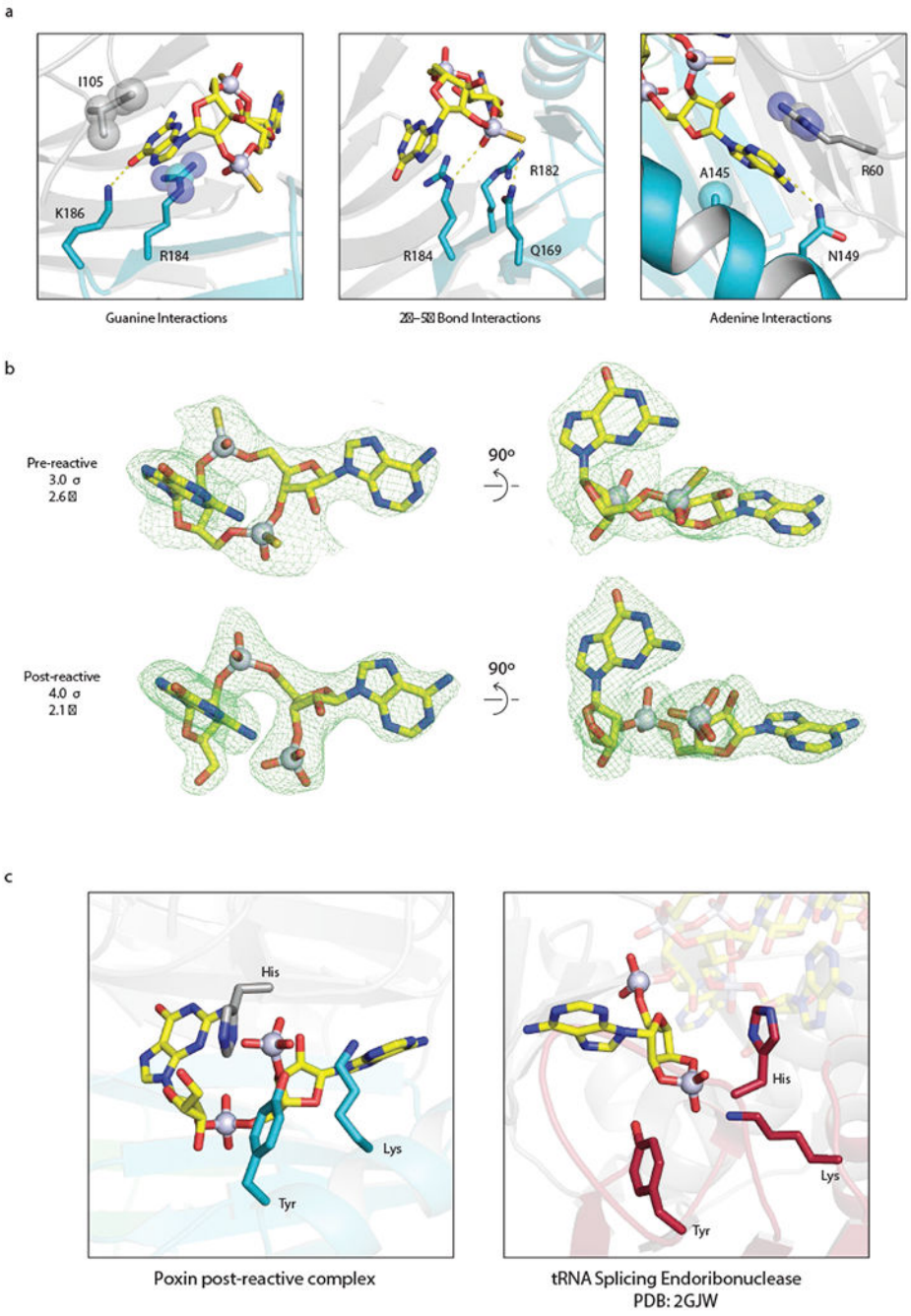

Extended Data Figure 6 |. Structural analysis of poxin 2′3′ cGAMP binding.

a, Overview of interactions in the VACV poxin–2′3′ cGAMP complex that mediate substrate specificity. VACV poxin residues make three types of interactions with 2′3′ cGAMP: sequence-specific contacts with the guanine base (left), hydrogen-bonding interactions with the 2′–5′ bond (middle), and sequence non-specific contacts with the adenine base (right). **b**, Simulated annealing omit maps showing electron density of 2′3′ cGAMP before and after poxin cleavage. Base identities can clearly be assigned in both pre- and post-reactive structures. A clear gap exists in the post-reactive structure between the

guanine 5′ OH and adenine 3′ phosphate confirming the poxin product is Gp[2′–5′]Ap[3′]. **c**, tRNA splicing endoribonucleases are metal-independent enzymes that degrade ribonucleotide substrates through a 2′–3′ cyclic phosphate intermediate. These enzymes share the poxin catalytic triad composed of histidine, tyrosine, and lysine, suggesting a related catalytic mechanism, despite the lack of sequence or structural homology.

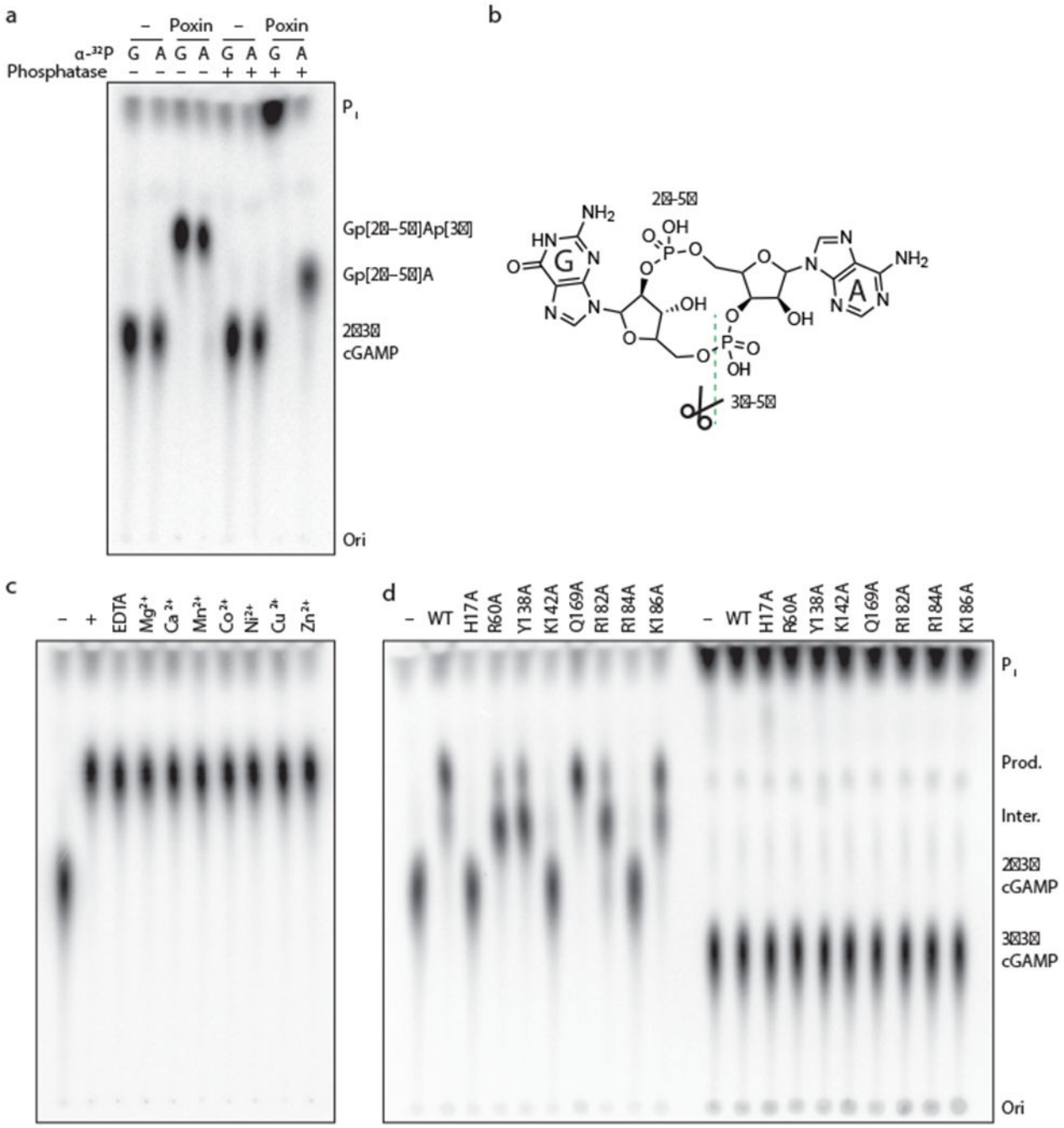

Extended Data Figure 7 |. VACV poxin degrades 2′3′ cGAMP through hydrolysis of the 3′–5′ bond.

a, TLC analysis of poxin activity using 2′3′ cGAMP radiolabeled at the 2′–5′ (α^{32}P A) or 3′–5′ (α^{32}P G) phosphodiester bonds. Radiolabeled 2′3′ cGAMP was incubated with recombinant VACV poxin and then treated with phosphatase to remove exposed phosphates from the final product. Following hydrolysis, the guanosine phosphate is exposed for phosphatase removal confirming the structural findings that VACV poxin specifically cleaves the 3′–5′ linkage of 2′3′ cGAMP. **b**, Schematic of VACV poxin induced hydrolysis

of 2′3′ cGAMP. **c**, TLC analysis of VACV poxin 2′3′ cGAMP degradation activity in the presence of 5 mM EDTA metal chelation or divalent cation supplementation. Divalent cations were supplemented at the following concentrations: 5 mM Mg^{2+}, 5 mM Ca^{2+}, 1 mM Mn^{2+}, 1 μM Co^{2+}, 1 μM Ni^{2+}, 1 μM Cu^{2+}, 1 μM Zn^{2+}. Poxin activity is resistant to EDTA, and divalent cations have no effect on the reaction, confirming the structural findings that VACV poxin activity is metal-independent. **d**, TLC analysis of VACV poxin active site mutants incubated for 20 h with 2′3′ cGAMP or 3′3′ cGAMP, demonstrating that all active site mutants retain specificity for 2′3′ cGAMP. All data are representative of 3 independent experiments.

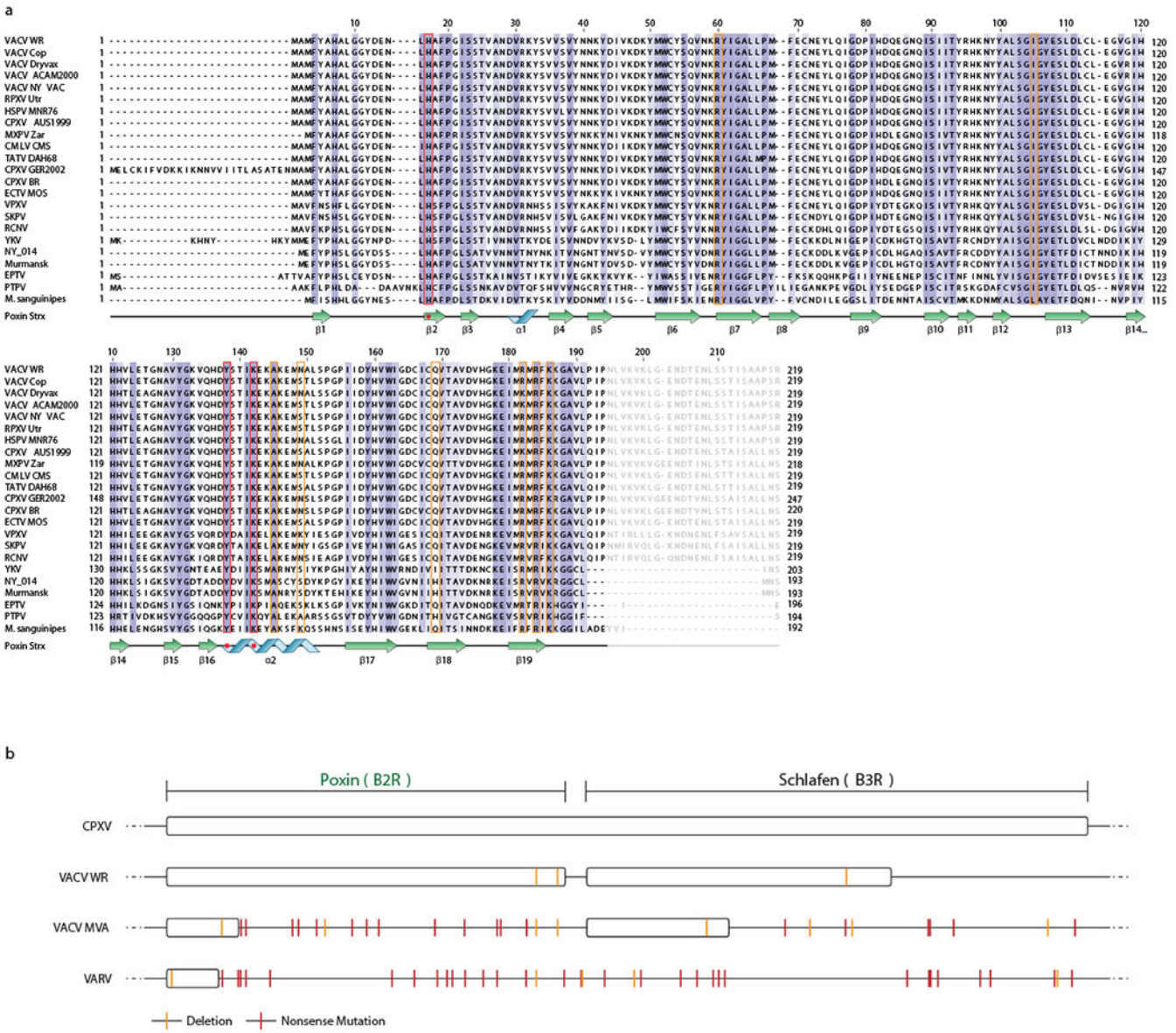

Extended Data Figure 8 |. Alignment of poxin proteins conserved in poxvirus representatives.

a, The poxin protein is highly conserved in mammalian poxviruses. The alignment is shaded according to conservation of physiochemical amino acid property, and numbered above according the VACV poxin amino acid sequence. The determined VACV poxin secondary structure is depicted below, active-site residues are indicated with a red dot and boxed in red, and residues that contact 2′3′ cGAMP are boxed in orange. VACV poxin residues 195–219 are not observed in the crystal structure. Sequences depicted in alignment are as follows: VACV WR (Vaccina virus strain Western Reserve, accession YP_233066.1), VACV Cop (Vaccinia virus strain Copenhagen, accession P20999.1), VACV Dryvax (Vaccinia virus strain Dryvax, accession AEY73716.1), VACV ACAM2000 (Vaccinia virus strain ACAM2000, accession AAQ93281.1), VACV NYVAC (Vaccinia virus strain NYVAC), RPXV Utr (rabbit poxvirus strain Utrecht, accession AY484669.1), HSPV MNR76 (horsepox virus strain MNR76, accession ABH08291.1), CPXV AUS1999 (cowpox virus

strain AUS1999, accession ADZ24189.1), MPXV ZAR (monkeypox virus strain Zaire-96-I-16, accession NP_536592.1), CMLV CMS (camelpox virus strain CMS, accession AAG37679.1), TATV DAH68 (taterapox virus strain Dahomey 1968, accession YP_717493.1), CPXV GER2002 (cowpox virus strain GER2002, accession ADZ30373.1), CPXV BR (cowpox virus strain Brighton Red, accession NP_619978.1), ECTV MOS (ectromelia virus strain Moscow, accession NP_671672.1), VPXV (volepox virus, accession YP_009281928.1), SKPV (skunkpox virus, accession YP_009282874.1), RCNV (racoonpox virus, accession YP_009143488.1), YKV (yokapox virus, accession YP_004821513.1), NY_014 (NY_014 virus, accession YP_009408559.1), Murmansk (Murmansk poxvirus, accession YP_009408359.1), EPTV (Eptesipoxvirus [*Eptesicus fuscus*], accession YP_009408111.1), PTPV (*Pteropus scapulatus*, accession YP_009268718.1), *M. sanguinipes* (*M. sanguinipes* entomopox virus, accession NP_048308.1). **b**, Schematized alignment of poxvirus genomic DNA showing the poxin *B2R / B3R* locus. White boxes indicate predicted open reading frames beginning with the annotated start codons and ending with the first stop codon, deletion and nonsense mutations are shown as orange and red bars. CPXV encodes an intact poxin–schlafen fusion protein, whereas the VACV genome contains a stop codon immediately following the poxin coding region and a frameshift mutation in the schlafen (*B3R*) gene. Poxin is inactivated in MVA and VARV by serial mutation.

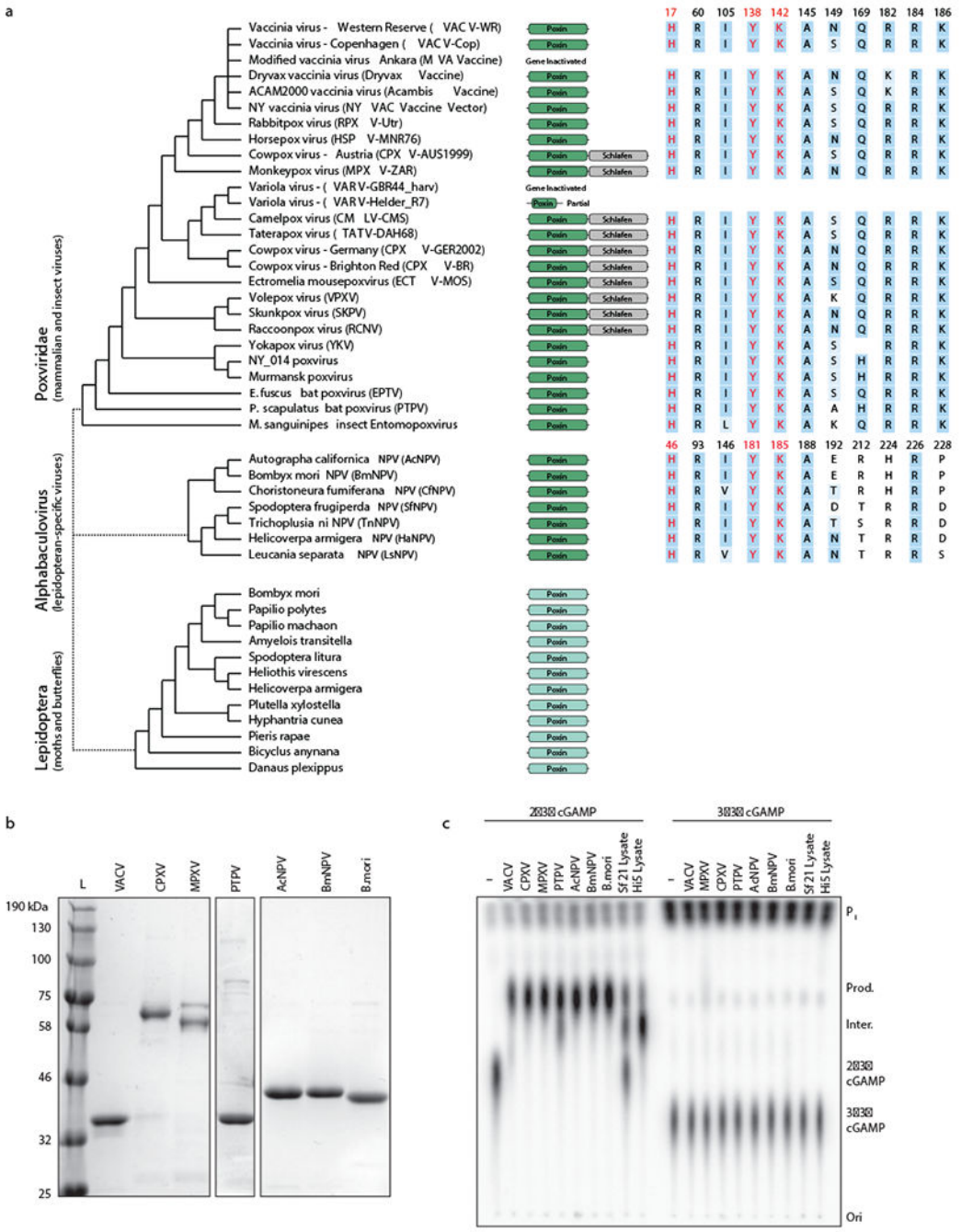

Extended Data Figure 9 |. Conservation of poxin family members and 2′3′ cGAMP-specific nuclease activity in *Poxviridae*, *Baculoviridae*, and host *Lepidoptera*.

a, Phylogenetic conservation of poxin family members in *Poxviridae*, *Baculoviridae*, and host *Lepidoptera* genomes. Poxin catalytic (red) and 2′3′ cGAMP interacting residues (black) are indicated on the right, shaded in blue according to conservation, and listed according to VACV poxin amino acid number (*Poxviridae*, top) or *AcNPV* poxin amino-acid number (*Baculoviridae*, middle). The metazoan poxin sequences from moth and butterfly genomes (*Lepidoptera*, bottom) share homology throughout the entire poxin protein and

exhibit identical 2′3′ cGAMP degradation activity, but the alignment with viral poxins does not allow definitive assignment of the catalytic residues. Phylogram schematics are based on previous analyses[52–55]. **b**, Coomasie-stained SDS-PAGE analysis of recombinant SUMO2-tagged poxin homologue proteins. **c**, TLC analysis of recombinant viral and host cellular poxin activity after 20 h incubation with substrates. All viral and metazoan poxin family members are exquisitely specific 2′3′ cGAMP nucleases. No activity is detected using the chemically related cyclic dinucleotide 3′3′ cGAMP. Data are representative of 3 independent experiments.

Extended Data Table 1 | Summary of data collection, phasing and refinement statistics.

All datasets were collected from individual crystals. Values in parentheses are for the highest resolution shell.

	SeMet-VACV Poxin *Apo* (6EA6)	VACV Poxin Pre-reactive State (6EA8)	VACV Poxin Post-reactive State (6EA9)
Data collection			
Space group	P 1 2_1 1	P 1 2_1 1	C 1 2 1
Cell dimensions			
a, *b*, *c* (Å)	55.0, 93.2, 94.1	59.4, 92.3, 257.1	215.4, 57.2, 133.1
α, *β*, *γ* (°)	90.0, 105.63, 90.0	90.0, 93.7, 90.0	90.0, 120.4, 90.0
Wavelength	0.97920 Å	0.97918	0.97918
Resolution (Å)	46.60–1.70 (1.73–1.70)	49.48–2.60 (2.65–2.60)	38.28–2.10 (2.14–2.10)
R_{pim}	4.9 (64.2)	5.1 (84.4)	3.5 (68.1)
$I/\sigma(I)$	20.3 (1.5)	9.3 (1.2)	9.9 (1.1)
$CC_{1/2}$	93.0 (55.8)	91.9 (34.8)	99.9 (84.7)
Completeness (%)	99.3 (89.6)	99.0 (97.7)	99.2 (97.2)
Redundancy	38.6 (22.6)	3.0 (3.0)	3.5 (3.2)
Refinement			
Resolution (Å)	46.60–1.70	49.48–2.60	38.28–2.1
No. reflections			
Total	3,858,564	252,224	288,415
Unique	99,918 (4,418)	84,690 (4,369)	81,341 (4,327)
Free (%)	2.1	2.3	2.5
R_{work} / R_{free}	15.99 / 18.22	21.77 / 25.23	19.94 / 23.39
No. atoms			
Protein	6160	15,319	7,762
Ligand		136	230
Water	750	156	202
B factors			
Protein	29.92	96.31	66.28
Ligand		109.63	59.71
Water	40.74	59.07	52.00
r.m.s deviations			

	SeMet-VACV Poxin *Apo* (6EA6)	VACV Poxin Pre-reactive State (6EA8)	VACV Poxin Post-reactive State (6EA9)
Bond lengths (Å)	0.012	0.004	0.007
Bond angles (°)	1.39	0.93	1.13

Supplementary Material

Refer to Web version on PubMed Central for supplementary material.

Acknowledgements:

The authors acknowledge A. Lee, K. Chat, R. Vance, S. Whelan, D. Knipe, V. Brusic, M. Bakkers, and members of the Kranzusch lab for helpful comments and discussion, and all collaborators for generously sharing virus-infected cells. We thank W. Zhou, B. Lowey, and K. McCarty for assistance with protein purification, R. Tomaino and the Harvard Medical School Taplin Mass Spectrometry Facility, and C. Miller for assistance with X-ray data collection. The work was funded by the Claudia Adams Barr Program for Innovative Cancer Research (P.J.K.), Richard and Susan Smith Family Foundation (P.J.K.), Charles H. Hood Foundation (P.J.K.), a Cancer Research Institute CLIP Grant (P.J.K.), funding from the Parker Institute for Cancer Immunotherapy (P.J.K.), NIH grants R01 AI127654 and R01 AR062807 (T.S.K.), and support through an NIH T32 Training Grant AI007245 (J.B.E.). X-ray data were collected the Lawrence Berkeley National Lab Advanced Light Source beamline 8.2.1, and at the Northeastern Collaborative Access Team beamline 24-ID-C, which are funded by the NIGMS (P30 GM124165, P41 GM103403) and an NIH-ORIP HEI grant (S10 RR029205) and used resources of the DOE Argonne National Laboratory Advanced Photon Source (under Contract No. DE-AC02-06CH11357).

References

1. Ablasser A et al. cGAS produces a 2’-5’-linked cyclic dinucleotide second messenger that activates STING. Nature 498, 380–384, doi:10.1038/nature12306 (2013). [PubMed: 23722158]
2. Diner EJ et al. The innate immune DNA sensor cGAS produces a noncanonical cyclic dinucleotide that activates human STING. Cell Rep 3, 1355–1361, doi:10.1016/j.celrep.2013.05.009 (2013). [PubMed: 23707065]
3. Gao P et al. Cyclic [G(2’,5’)pA(3’,5’)p] is the metazoan second messenger produced by DNA-activated cyclic GMP-AMP synthase. Cell 153, 1094–1107, doi:10.1016/j.cell.2013.04.046 (2013). [PubMed: 23647843]
4. Sun L, Wu J, Du F, Chen X & Chen ZJ Cyclic GMP-AMP synthase is a cytosolic DNA sensor that activates the type I interferon pathway. Science 339, 786–791, doi:10.1126/science.1232458 (2013). [PubMed: 23258413]
5. Ablasser A et al. Cell intrinsic immunity spreads to bystander cells via the intercellular transfer of cGAMP. Nature 503, 530–534, doi:10.1038/nature12640 (2013). [PubMed: 24077100]
6. Li L et al. Hydrolysis of 2’3’-cGAMP by ENPP1 and design of nonhydrolyzable analogs. Nat Chem Biol 10, 1043–1048, doi:10.1038/nchembio.1661 (2014). [PubMed: 25344812]
7. Wu J & Chen ZJ Innate immune sensing and signaling of cytosolic nucleic acids. Annu Rev Immunol 32, 461–488, doi:10.1146/annurev-immunol-032713-120156 (2014). [PubMed: 24655297]
8. Bridgeman A et al. Viruses transfer the antiviral second messenger cGAMP between cells. Science 349, 1228–1232, doi:10.1126/science.aab3632 (2015). [PubMed: 26229117]
9. Gentili M et al. Transmission of innate immune signaling by packaging of cGAMP in viral particles. Science 349, 1232–1236, doi:10.1126/science.aab3628 (2015). [PubMed: 26229115]
10. Bidgood SR & Mercer J. Cloak and Dagger: Alternative Immune Evasion and Modulation Strategies of Poxviruses. Viruses 7, 4800–4825, doi:10.3390/v7082844 (2015). [PubMed: 26308043]
11. Schoggins JW et al. Pan-viral specificity of IFN-induced genes reveals new roles for cGAS in innate immunity. Nature 505, 691–695, doi:10.1038/nature12862 (2014). [PubMed: 24284630]

12. Dai P et al. Modified vaccinia virus Ankara triggers type I IFN production in murine conventional dendritic cells via a cGAS/STING-mediated cytosolic DNA-sensing pathway. PLoS pathogens 10, e1003989, doi:10.1371/journal.ppat.1003989 (2014). [PubMed: 24743339]
13. Georgana I, Sumner RP, Towers GJ & Maluquer de Motes C Virulent poxviruses inhibit DNA sensing by preventing STING activation. J Virol, doi:10.1128/jvi.02145-17 (2018).
14. Cheng WY et al. The cGas-Sting Signaling Pathway Is Required for the Innate Immune Response Against Ectromelia Virus. Frontiers in immunology 9, 1297, doi:10.3389/fimmu.2018.01297 (2018). [PubMed: 29963044]
15. Shi H, Wu J, Chen ZJ & Chen C Molecular basis for the specific recognition of the metazoan cyclic GMP-AMP by the innate immune adaptor protein STING. Proc Natl Acad Sci U S A 112, 8947–8952, doi:10.1073/pnas.1507317112 (2015). [PubMed: 26150511]
16. Gao P et al. Structure-function analysis of STING activation by c[G(2',5')pA(3',5')p] and targeting by antiviral DMXAA. Cell 154, 748–762, doi:10.1016/j.cell.2013.07.023 (2013). [PubMed: 23910378]
17. Zhang X et al. Cyclic GMP-AMP containing mixed phosphodiester linkages is an endogenous high-affinity ligand for STING. Mol Cell 51, 226–235, doi:10.1016/j.molcel.2013.05.022 (2013). [PubMed: 23747010]
18. Kranzusch PJ et al. Ancient Origin of cGAS-STING Reveals Mechanism of Universal 2',3' cGAMP Signaling. Mol Cell 59, 891–903, doi:10.1016/j.molcel.2015.07.022 (2015). [PubMed: 26300263]
19. Xue S, Calvin K & Li H RNA recognition and cleavage by a splicing endonuclease. Science 312, 906–910, doi:10.1126/science.1126629 (2006). [PubMed: 16690865]
20. Yang W Nucleases: diversity of structure, function and mechanism. Q Rev Biophys 44, 1–93, doi: 10.1017/S0033583510000181 (2011). [PubMed: 20854710]
21. Liu F, Zhou P, Wang Q, Zhang M & Li D The Schlafen family: complex roles in different cell types and virus replication. Cell Biol Int 42, 2–8, doi:10.1002/cbin.10778 (2018). [PubMed: 28460425]
22. Liu Y et al. Inflammation-Induced, STING-Dependent Autophagy Restricts Zika Virus Infection in the Drosophila Brain. Cell Host Microbe 24, 57–68 e53, doi:10.1016/j.chom.2018.05.022 (2018). [PubMed: 29934091]
23. Martin M, Hiroyasu A, Guzman RM, Roberts SA & Goodman AG Analysis of Drosophila STING Reveals an Evolutionarily Conserved Antimicrobial Function. Cell Rep 23, 3537–3550 e3536, doi: 10.1016/j.celrep.2018.05.029 (2018). [PubMed: 29924997]
24. Shin SW et al. Isolation and characterization of immune-related genes from the fall webworm, Hyphantria cunea, using PCR-based differential display and subtractive cloning. Insect Biochem Mol Biol 28, 827–837 (1998). [PubMed: 9818384]
25. Elde NC et al. Poxviruses deploy genomic accordions to adapt rapidly against host antiviral defenses. Cell 150, 831–841, doi:10.1016/j.cell.2012.05.049 (2012). [PubMed: 22901812]
26. Theze J, Takatsuka J, Nakai M, Arif B & Herniou EA Gene acquisition convergence between entomopoxviruses and baculoviruses. Viruses 7, 1960–1974, doi:10.3390/v7041960 (2015). [PubMed: 25871928]
27. Meade N et al. Poxviruses Evade Cytosolic Sensing through Disruption of an mTORC1-mTORC2 Regulatory Circuit. Cell 174, 1143–1157 e1117, doi:10.1016/j.cell.2018.06.053 (2018). [PubMed: 30078703]
28. Kim M Replicating poxviruses for human cancer therapy. J Microbiol 53, 209–218, doi:10.1007/s12275-015-5041-4 (2015). [PubMed: 25845536]
29. Moss B Reflections on the early development of poxvirus vectors. Vaccine 31, 4220–4222, doi: 10.1016/j.vaccine.2013.03.042 (2013). [PubMed: 23583893]
30. Ma Z & Damania B The cGAS-STING Defense Pathway and Its Counteraction by Viruses. Cell Host Microbe 19, 150–158, doi:10.1016/j.chom.2016.01.010 (2016). [PubMed: 26867174]

Extended References

31. Fuerst TR, Niles EG, Studier FW & Moss B Eukaryotic transient-expression system based on recombinant vaccinia virus that synthesizes bacteriophage T7 RNA polymerase. Proc Natl Acad Sci U S A 83, 8122–8126 (1986). [PubMed: 3095828]
32. Cotter CA, Earl PL, Wyatt LS & Moss B Preparation of Cell Cultures and Vaccinia Virus Stocks. Current protocols in protein science 89, 5.12.11–15.12.18, doi:10.1002/cpps.34 (2017).
33. Zhou W et al. Structure of the Human cGAS-DNA Complex Reveals Enhanced Control of Immune Surveillance. Cell 174, 300–311 e311, doi:10.1016/j.cell.2018.06.026 (2018). [PubMed: 30007416]
34. Kranzusch PJ et al. Structure-guided reprogramming of human cGAS dinucleotide linkage specificity. Cell 158, 1011–1021, doi:10.1016/j.cell.2014.07.028 (2014). [PubMed: 25131990]
35. Reverter D & Lima CD Structural basis for SENP2 protease interactions with SUMO precursors and conjugated substrates. Nat Struct Mol Biol 13, 1060–1068, doi:10.1038/nsmb1168 (2006). [PubMed: 17099700]
36. Lee AS, Kranzusch PJ & Cate JH eIF3 targets cell-proliferation messenger RNAs for translational activation or repression. Nature 522, 111–114, doi:10.1038/nature14267 (2015). [PubMed: 25849773]
37. Kranzusch PJ, Lee AS, Berger JM & Doudna JA Structure of human cGAS reveals a conserved family of second-messenger enzymes in innate immunity. Cell Rep 3, 1362–1368, doi:10.1016/j.celrep.2013.05.008 (2013). [PubMed: 23707061]
38. Olson AT, Rico AB, Wang Z, Delhon G & Wiebe MS Deletion of the Vaccinia Virus B1 Kinase Reveals Essential Functions of This Enzyme Complemented Partly by the Homologous Cellular Kinase VRK2. J Virol 91, doi:10.1128/jvi.00635-17 (2017).
39. Pedelacq JD, Cabantous S, Tran T, Terwilliger TC & Waldo GS Engineering and characterization of a superfolder green fluorescent protein. Nature biotechnology 24, 79–88, doi:10.1038/nbt1172 (2006).
40. Roper RL Rapid preparation of vaccinia virus DNA template for analysis and cloning by PCR. Methods in molecular biology (Clifton, N.J.) 269, 113–118, doi:10.1385/1-59259-789-0:113 (2004).
41. Orzalli MH et al. cGAS-mediated stabilization of IFI16 promotes innate signaling during herpes simplex virus infection. Proc Natl Acad Sci U S A 112, E1773–1781, doi:10.1073/pnas.1424637112 (2015). [PubMed: 25831530]
42. Arezi B & Hogrefe H Novel mutations in Moloney Murine Leukemia Virus reverse transcriptase increase thermostability through tighter binding to template-primer. Nucleic acids research 37, 473–481, doi:10.1093/nar/gkn952 (2009). [PubMed: 19056821]
43. Jiang X et al. Skin infection generates non-migratory memory CD8+ T(RM) cells providing global skin immunity. Nature 483, 227–231, doi:10.1038/nature10851 (2012). [PubMed: 22388819]
44. Pan Y et al. Survival of tissue-resident memory T cells requires exogenous lipid uptake and metabolism. Nature 543, 252–256, doi:10.1038/nature21379 (2017). [PubMed: 28219080]
45. Kabsch W Xds. Acta Crystallogr D Biol Crystallogr 66, 125–132, doi:10.1107/S0907444909047337 (2010). [PubMed: 20124692]
46. Adams PD et al. PHENIX: a comprehensive Python-based system for macromolecular structure solution. Acta Crystallogr D Biol Crystallogr 66, 213–221, doi:10.1107/S0907444909052925 (2010). [PubMed: 20124702]
47. Terwilliger TC Reciprocal-space solvent flattening. Acta Crystallogr D Biol Crystallogr 55, 1863–1871 (1999). [PubMed: 10531484]
48. Emsley P & Cowtan K Coot: model-building tools for molecular graphics. Acta Crystallogr D Biol Crystallogr 60, 2126–2132, doi:10.1107/S0907444904019158 (2004). [PubMed: 15572765]
49. Fernandes H, Leen EN, Cromwell H Jr., Pfeil MP & Curry S Structure determination of Murine Norovirus NS6 proteases with C-terminal extensions designed to probe protease-substrate interactions. PeerJ 3, e798, doi:10.7717/peerj.798 (2015). [PubMed: 25755927]
50. Katz BA et al. Elaborate manifold of short hydrogen bond arrays mediating binding of active site-directed serine protease inhibitors. J Mol Biol 329, 93–120 (2003). [PubMed: 12742021]

51. Holm L & Laakso LM Dali server update. Nucleic acids research 44, W351–355, doi:10.1093/nar/gkw357 (2016). [PubMed: 27131377]

52. Jacob JM et al. Complete genome sequence of a novel sea otterpox virus. Virus genes 54, 756–767, doi:10.1007/s11262-018-1594-8 (2018). [PubMed: 30225673]

53. Smithson C et al. Two novel poxviruses with unusual genome rearrangements: NY_014 and Murmansk. Virus genes 53, 883–897, doi:10.1007/s11262-017-1501-8 (2017). [PubMed: 28762208]

54. Theze J, Lopez-Vaamonde C, Cory JS & Herniou EA Biodiversity, Evolution and Ecological Specialization of Baculoviruses: A Treasure Trove for Future Applied Research. Viruses 10, doi:10.3390/v10070366 (2018).

55. Mitter C, Davis DR & Cummings MP Phylogeny and Evolution of Lepidoptera. Annual review of entomology 62, 265–283, doi:10.1146/annurev-ento-031616-035125 (2017).

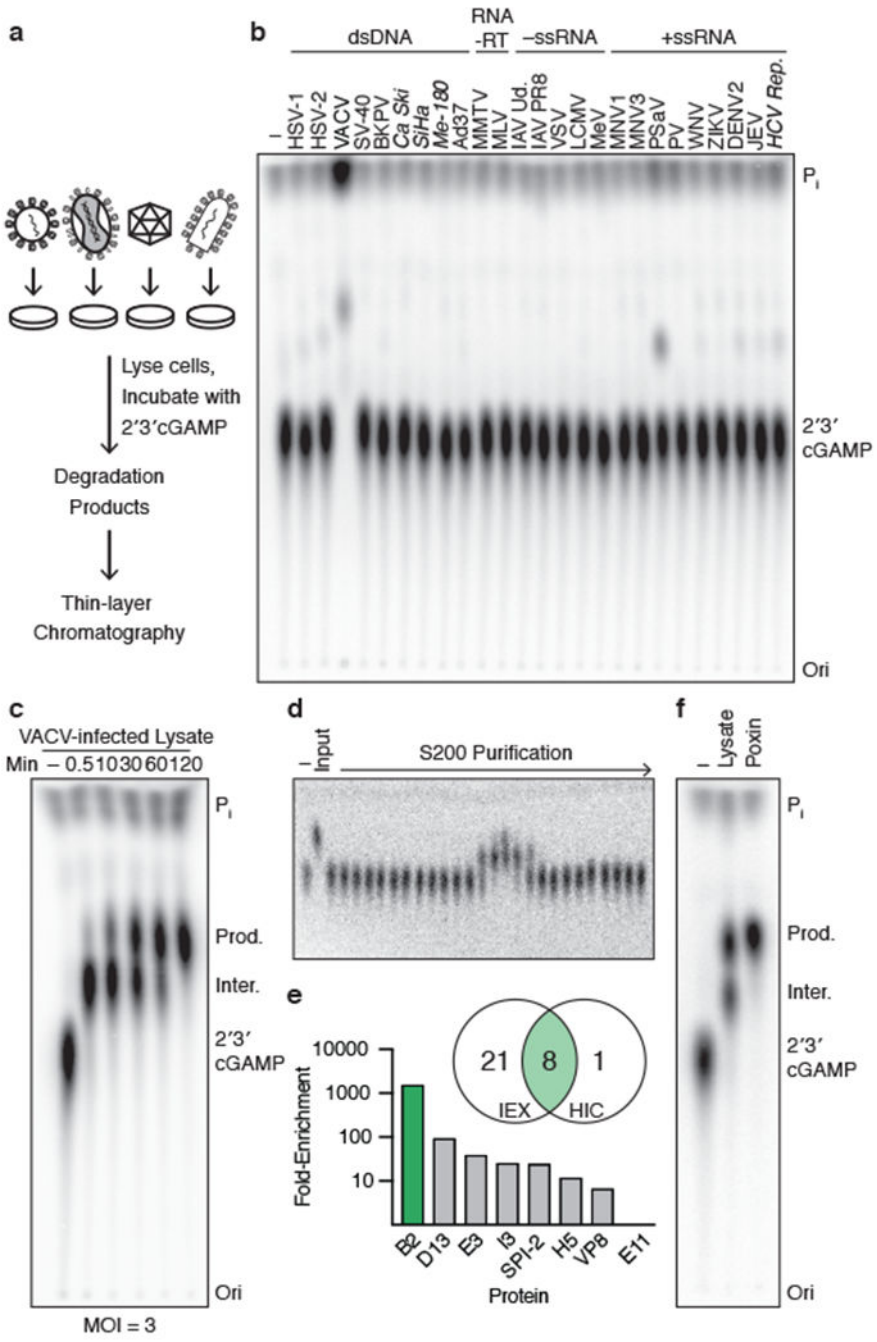

Figure 1 |. A poxvirus nuclease disrupts 2′3′ cGAMP immune signaling.

a, **b**, Thin-layer chromatography (TLC) analysis of 2′3′ cGAMP degradation following 20 h incubation in lysates derived from virus-infected or virus protein-expressing cells. Vaccinia virus (VACV) infection induces degradation of 2′3′ cGAMP. **c**, VACV-infected cell lysate rapidly degrades 2′3′ cGAMP in <30 s to an intermediate product and then to a fast-migrating final product. **d, e**, Activity-guided fractionation from VACV-infected cell lysate and mass spectrometry of enriched proteins identifies the VACV *B2R* gene product (green) as the poxin protein. **f,** Analysis of 2′3′ cGAMP degradation comparing VACV-

infected cell lysates and recombinant poxin produced in *E. coli*. All data are representative of at least 2 independent experiments.

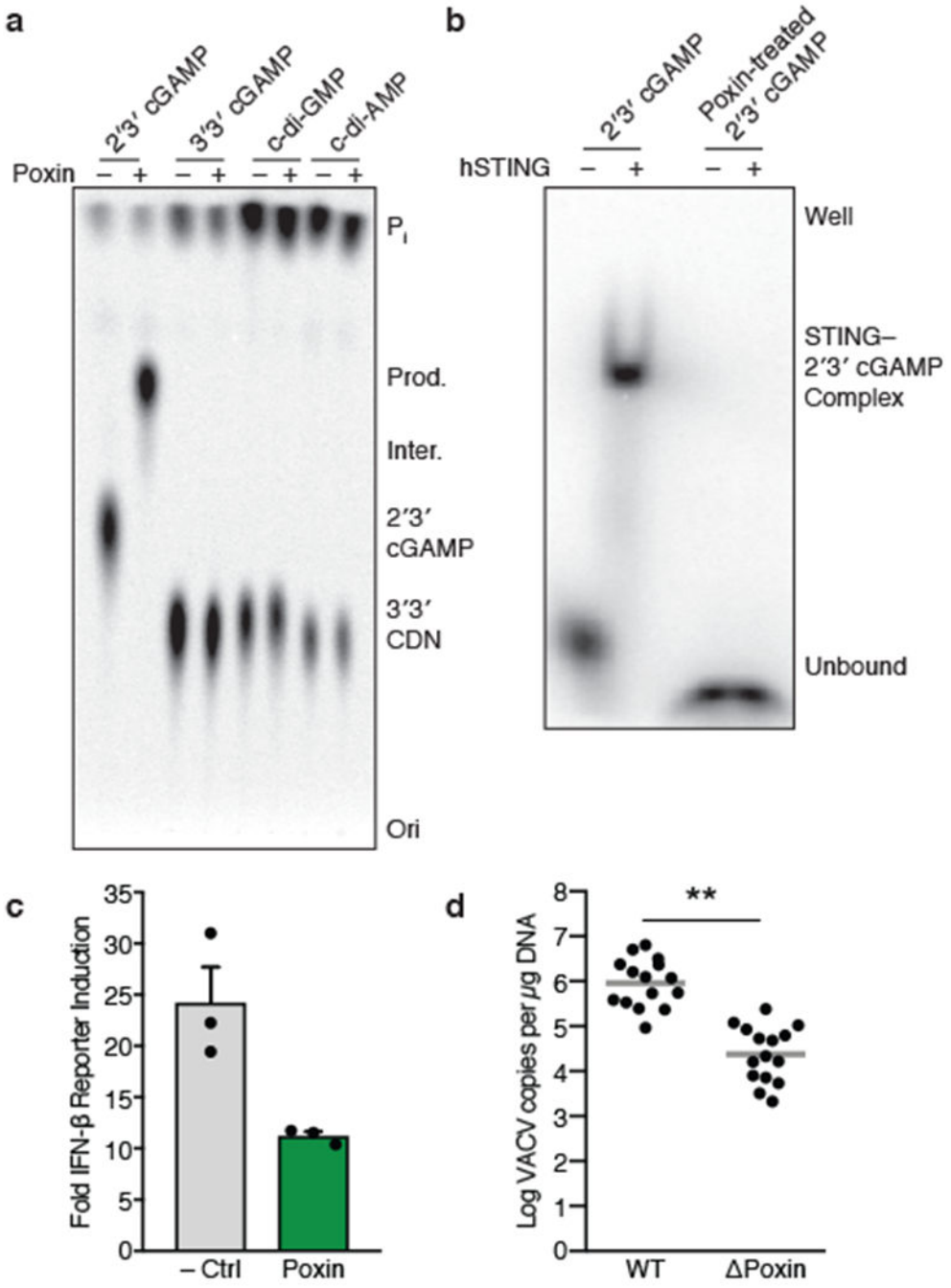

Figure 2 |. VACV poxin is critical for evasion of cGAS-STING immunity.

a, VACV poxin is specific for 2′3′ cGAMP and fails to degrade 3′3′ cGAMP or other natural cyclic dinucleotide (CDN) species. **b**, Human STING electrophoretic mobility shift assay showing poxin degradation of 2′3′ cGAMP blocks the interaction with STING required for downstream immune activation. **c**, Cells expressing VACV poxin have a dampened response to cGAS-dependent activation of an interferon-β reporter compared with cells expressing a catalytically inactive poxin mutant (H17A, −Ctrl). Data are +/− SEM of three technical replicates and are representative of three independent experiments. **d,** Mice

were infected via scarification with wildtype VACV or a poxin knockout strain (ΔPoxin). Clearance of VACV-ΔPoxin in the skin is enhanced >40-fold (**, Student's t-test, two-tailed $p = 4.01 \times 10^{-8}$) compared to wildtype. Black dots represent individual mice and grey bars designate the mean value of each group (n = 15). All data are representative of at least 2 independent experiments.

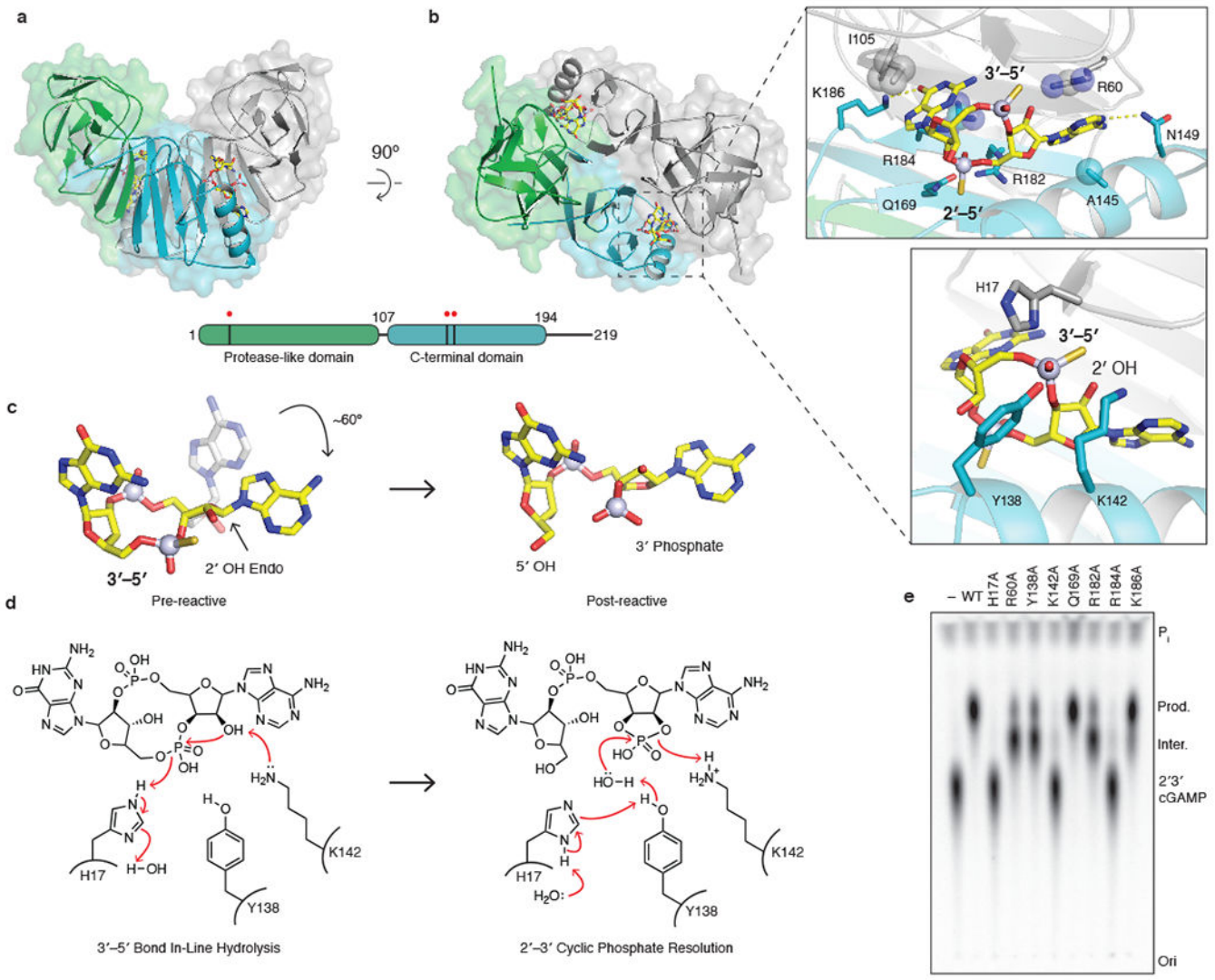

Figure 3 |. Structural basis of poxin activity and mechanism of 2′3′ cGAMP degradation.

a, Crystal structure of VACV poxin bound to 2′3′ cGAMP. Poxin is a homodimer with two active sites formed at the interfaces of an N-terminal protease-like domain (green) and C-terminal domain (cyan) from apposing monomers. Schematic denotes poxin domain organization and location of active site residues (red dots). **b**, Top-down view of the VACV poxin–2′3′ cGAMP complex. Cutaways show the pre-reactive complex and highlight residues involved in 2′3′ cGAMP recognition (top) and 3′–5′ bond hydrolysis (bottom). **c**,**d,** Conformation of 2′3′ cGAMP bound to poxin in the pre-reactive and post-reactive states, and mechanism of poxin metal-independent hydrolysis. **e**, Analysis of 2′3′ cGAMP degradation using recombinant poxin protein with mutations to key active site residues. Data are representative of 3 independent experiments.

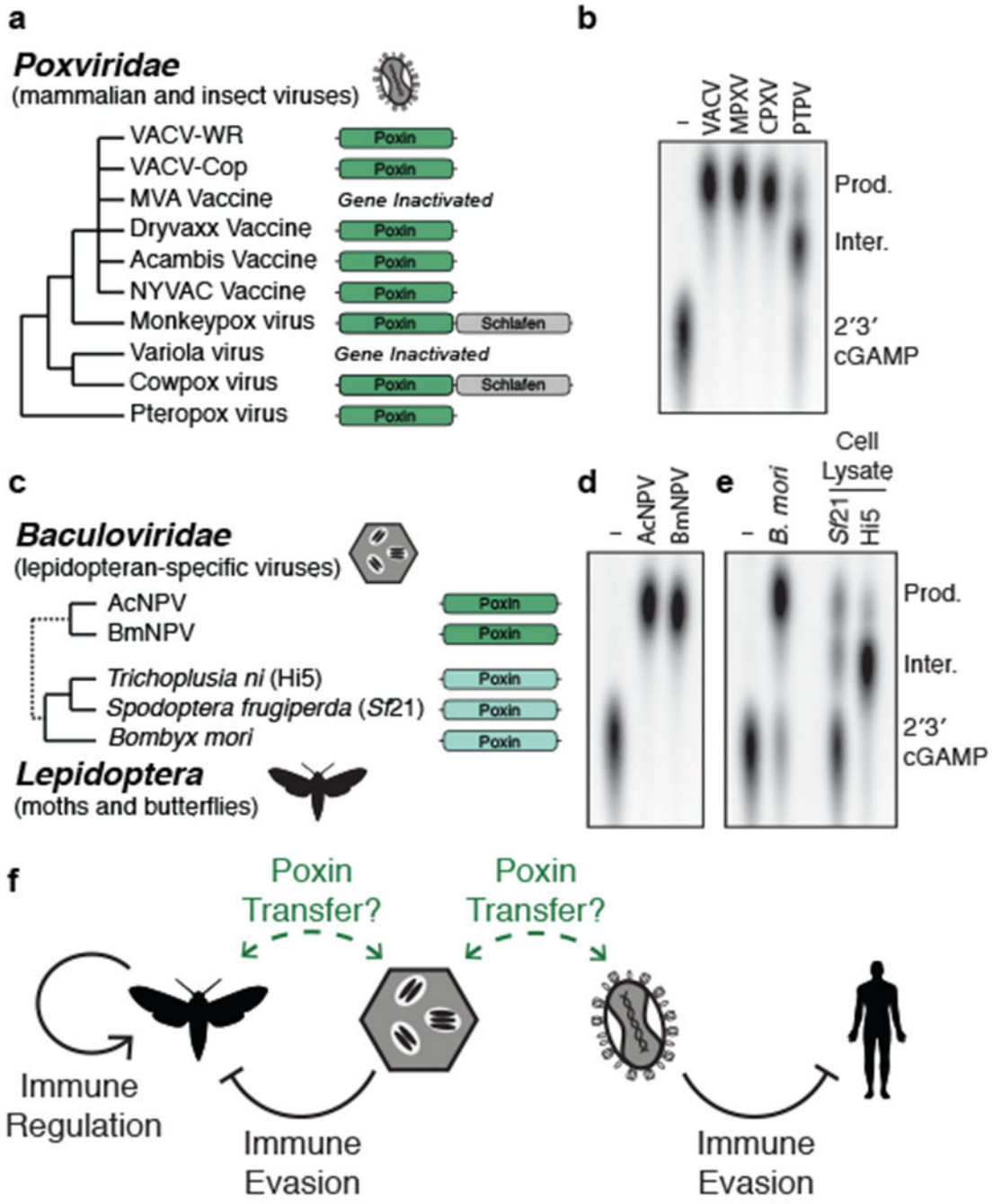

Figure 4 |. Discovery of viral and host cellular poxin homologues.

a, Schematic of poxin conservation in the *Poxviridae*, and **b**, analysis confirming these poxin homologues retain 2′3′ cGAMP hydrolysis activity. **c**, Phylogenetic schematic depicting identification of insect viral poxin homologues in the family *Baculoviridae* and host cellular poxin homologues in moth and butterfly genomes. **d**,**e**, Recombinant protein analysis as in (**b**) demonstrating that insect viral and insect cellular poxin proteins retain specific 2′3′ cGAMP degradation activity. Poxin activity is detected in the lysates of common lepidopteran cell lines *Sf*21 and Hi5. **f**, Schematic of one possible evolutionary path of

emergence of poxin immune evasion in mammalian viruses. All data are representative of 3 independent experiments.